Full Title:

Multiple molecular events underlie stochastic switching between two heritable cell states in a eukaryotic system

Short Title:

Multiple molecular events underlie stochastic cell fate switching

Author list:

Naomi Ziv[1], Lucas R. Brenes[1,2], Alexander Johnson[1]

Author affiliations:

[1]Department of Microbiology and Immunology, University of California, San Francisco
[2]Current Address: Biology Graduate Program, Massachusetts Institute of Technology

Corresponding author:

Naomi Ziv: naomi.ziv@ucsf.edu
Alexander Johnson: ajohnson@cgl.ucsf.edu

Abstract

Eukaryotic transcriptional networks are often large and contain several levels of feedback regulation. Many of these networks have the ability to generate and maintain several distinct transcriptional states across multiple cell divisions and to switch between them. In certain instances, switching between cell states is stochastic, occurring in a small subset of cells of an isogenic population in a seemingly homogenous environment. Given the scarcity and unpredictability of switching in these cases, investigating the determining molecular events is challenging. White-opaque switching in the fungal species *Candida albicans* is an example of stably inherited cell states that are determined by a complex transcriptional network and can serve as an experimentally accessible model system to study characteristics important for stochastic cell fate switching in eukaryotes. In standard lab media, genetically identical cells maintain their cellular identity (either "white" or "opaque") through thousands of cell divisions and switching between the states is rare. By isolating populations of white or opaque cells, previous studies have elucidated the many differences between the two stable cell states and identified a set of transcriptional regulators needed for cell type switching. Yet little is known about the molecular events that determine the rare, stochastic switching events that occur in single cells. We use microfluidics combined with fluorescent reporters to directly observe rare switching events between the white and opaque states. We investigate the stochastic nature of switching by beginning with white cells and monitoring the activation of Wor1, a master regulator and marker for the opaque state, in single cells and throughout cell pedigrees. Our results indicate that switching requires two stochastic steps; first an event occurs that predisposes a lineage of cells to switch. In the second step, some but not all, of those predisposed cells rapidly express high levels of Wor1 and commit to the opaque state. To further understand the rapid rise in Wor1, we used a synthetic inducible system in *Saccharomyces cerevisiae* into which a controllable *C. albicans* Wor1 and a reporter for its transcriptional control region have been introduced. We document that Wor1 positive autoregulation is highly cooperative (Hill coefficient > 3), leading to rapid activation and producing an "all or none" rather than a graded response. Taken together, our results suggest that reaching a threshold level of a master regulator is sufficient to drive cell type switching in single cells and that an earlier molecular event increases the probability of reaching that threshold in certain small lineages of cells. Quantitative molecular analysis of the white-opaque circuit can serve as a model for the general understanding of complex circuits.

Introduction

Transcription circuits, defined as transcription regulators and the DNA cis-regulatory sequences they bind, control the expression of genes and thereby define cellular identity. Cellular identity is not static; gene expression programs change in response to external and internal stimuli. Certain transcriptional networks can produce distinct cell states that can be maintained through many cycles of cell division. The best-characterized of such circuits come from microbes, such as the cI-Cro circuit of phage lambda (Ptashne, 2011), the control of lactose utilization in *Escherichia coli* (Santillán & Mackey, 2008), competence in *Bacillus subtilis* (Maamar & Dubnau, 2005) and galactose utilization in *Saccharomyces cerevisiae* (Stockwell et al., 2015). Such "bistability" has also been engineered in both prokaryotic and eukaryotic synthetic circuits (Gardner et al., 2000; Kramer et al., 2004; Wu et al., 2013) and is thought to underlie many instances of cell differentiation in multicellular organisms (Chickarmane et al., 2006; Graham et al., 2010; Park et al., 2012). The production of two stable transcriptional states from a single genome depends on positive feedback regulation and non-linearity (such as cooperativity) within the feedback circuit, which can convert graded inputs into discontinuous switch-like outputs (Alon, 2007; Ferrell, 2002; Smits et al., 2006). The output of a given circuit "diagram" however, is entirely dependent on the physical parameters of the components, such as dissociation constants and protein concentrations; even slight variations in circuit architecture or parameters can produce distinct outputs (Çağatay et al., 2009). Many questions remain concerning the functional properties and parameters of network motifs found in real biological systems, particularly those based on the large regulatory networks commonly found in eukaryotic organisms. A major challenge to experimentally investigating the functional role of the multiple feedback loops present in complex circuits is the limited ability to independently manipulate the different components. In order to understand the output of these large networks, it is necessary to integrate the analysis of individual motifs with an analysis of the network as a whole.

In some cases, switching between states depends on external signals, but in other cases switching between stable states appears stochastic, occurring in a subset of cells of an isogenic population in a seemingly homogenous environment. In microbes, stochastic phenotypic switching is often thought of in terms of adaptation to fluctuating environments (Acar et al., 2008; Kussell, 2005b), where there is a predicted optimal relationship between the frequency of stochastic switching and the frequency of environmental change. In pathogens, stochastic switching can create distinct subpopulations with different cell features, protecting against targeted host defense systems (Norman et al., 2015). Stochastic switching also occurs during development to create cellular diversity (Losick & Desplan, 2008). For example, photoreceptor patterning in the fly retina is based on a choice between cell states following the stochastic expression of a single transcription factor (Wernet et al., 2006). Understanding stochastic phenotype switching at a molecular level is challenging, in particular, identifying the early, seemingly random, initiating events that determine which cells will undergo switching.

To study the mechanism of stochastic switching between two stable transcription states, we investigate white-opaque switching in *Candida albicans*, a common component of the human gut microbiota but also an opportunistic pathogen causing life-threatening bloodstream infections (Kim & Sudbery, 2011). White and opaque cells differ in the expression of hundreds of genes resulting in drastic differences in cell morphology, metabolism, the ability to mate and interactions with the immune system (Ene et al., 2016; Lohse & Johnson, 2009; Miller & Johnson, 2002; Sasse et al., 2013; Tuch et al., 2010). A complex transcriptional network controls white-opaque switching, as many (at least seven) transcription factors are involved and are known to regulate one another, in a series of nested feedback loops (Hernday et al., 2013; Lohse et al., 2016; Zordan et al., 2007). The master regulator of white-opaque switching is Wor1, a transcription factor whose deletion completely blocks switching (locking cells in the white state) and whose ectopic expression in white cells converts them *en masse* to opaque cells, even in the absence of other critical regulators (Lohse & Johnson, 2016; Zordan et al., 2006, 2007). Ectopic Wor1 expression activates expression from the endogenous Wor1 locus, which is necessary for maintaining the opaque cell state when ectopic expression is removed (Zordan et al., 2006). Wor1 is differently regulated between the two cell states, with 40-fold higher expression in opaque cells. In common with the other regulators of white-opaque switching, the Wor1 regulatory sequences (7KB upstream control region and 2KB 5'UTR) are some of the longest in the *C. albicans* genome (Tuch et al., 2010). Its complexity is reminiscent of enhancers from multicellular organisms, even exhibiting the phase transitions described for some mammalian enhancers (Frazer et al., 2020). Wor1 is positioned in the center of a network of multiple positive feedback loops, binding both its own promoter as well as those of both activators and repressors of the opaque cell state (Hernday et al., 2013; Zordan et al., 2007).

In this work, we investigate the process of white-opaque switching at a single cell level. To do so, we developed two complementary quantitative approaches to study the molecular mechanisms underlying switching. The first is the use of microfluidics and fluorescent microscopy to follow switching in *C. albicans*, allowing us to quantify the activation of the master regulator Wor1 in pedigrees where both switching and non-switching cells are dividing. The second is the use of a synthetic inducible system in *S. cerevisiae* to investigate the function of white-opaque regulators and characterize specific regulatory interactions, such as Wor1 autoregulation. Our results reveal features of white-opaque switching that were unanticipated from previous "bulk" culture analyses and provide key insights into the mechanism behind stochastic switching.

144 Results
145
146 *Observing white-opaque switching at a single cell level*
147
148 White-opaque switching has typically been studied by monitoring the formation of
149 colony sectors after plating single cells on solid agar and allowing them to grow and form
150 colonies of approximately 10^6 cells (FIGURE 1A, 1B, TABLE S1). A sector registers a
151 switching event that took place in the past and reveals the stochastic nature of switching
152 (e.g. sectors of different sizes in different colonies) but provides no insight into how the
153 original cell that founded the sector differed from the surrounding cells and underwent
154 switching. We set out to observe switching at a single cell level to understand how this
155 process occurs. Using switching competent *C. albicans* a/Δ diploid cells (METHODS),
156 we took advantage of microfluidic plates that contain specialized barrier traps (FIGURE
157 1C, METHODS). As the experiment begins, traps contain a few cells and, over time,
158 these cells divide, eventually filling the trap. After approximately 12 hours, each trap
159 holds ~400 cells. We continue imaging cells for an additional 12 hours, during which
160 cells continue to divide in the trap, pushing excess cells out of the trap where they flow
161 away. With this experimental set-up, we are able to observe thousands of divisions in
162 each trap and, by monitoring many traps, capture detailed instances of stochastic white-
163 opaque switching, even though these events are rare.
164
165 Wor1 is a master regulator of white-opaque switching and its expression is 40-fold higher
166 in opaque cells compared to white cells (Zordan et al., 2006). We followed switching
167 events in a strain homozygous for a Wor1-GFP fusion protein (FIGURE 1D, VIDEO 1).
168 Microfluidic experiments that began with cells from white colonies did not have any
169 visible GFP signal while those that began with cells from opaque colonies had uniformly
170 high levels of GFP signal (FIGURE 1D, FIGURE S1). Using this strain allowed for the
171 unambiguous identification of switching events as well as the quantification of the
172 increase in Wor1 expression as cells transition between the white and opaque states.
173 Although switching is still relatively rare and stochastic, strains containing the Wor1-
174 GFP fusion switch at higher rates than wildtype cells (TABLE S1), which enabled
175 observation of many independent switching events. GFP is known to form dimers at high
176 concentrations (Phillips, 1997; Yang et al., 1996) and when we introduced the GFP
177 A206K mutation (differentiated as mGFP below) to prevent dimerization (Zacharias,
178 2002), white-opaque switching reverted to wildtype levels (TABLE S1). By visualizing a
179 large number of traps, we were able to observe several switching events in the Wor1-
180 mGFP fusion strain. Apart from the difference in switching frequency, the switching
181 behavior (as described below) of the Wor1-mGFP fusion strain appeared identical to the
182 Wor1-GFP strain. Most of our data therefore was obtained from the elevated switching
183 strain with the low-switching strain used to validate it. As predicted from previous bulk
184 culture experiments, once the Wor1-GFP fusion reached a high level, it was faithfully
185 passed on to descendent cells, preserving the opaque state.

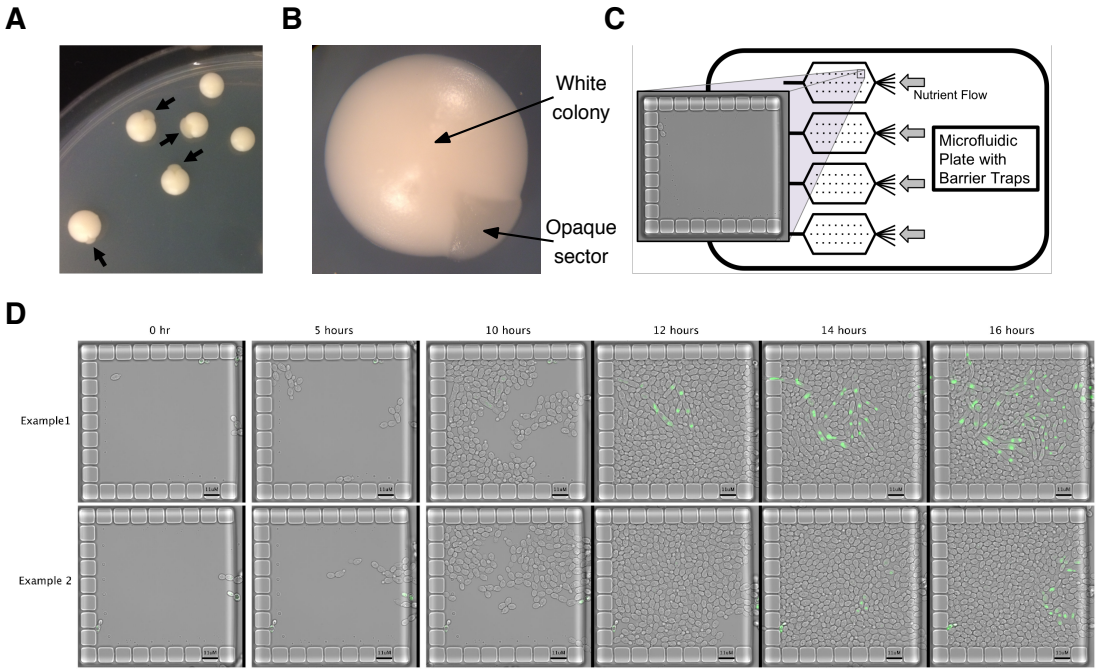

FIGURE 1 legend – Monitoring white-opaque switching in *Candida albicans*
A) Image of colonies produced by plating single white cells on solid agar. Arrows point to opaque sectors; each represents an independent switching event. This strain contains the Wor1-GFP fusion protein and hence exhibits higher than normal switching rates. B) Close up image of single white cell type colony with an opaque sector. C) Schematic of microfluidic plates used to study white-opaque switching at a single cell level. Each plate has four chambers; each chamber contains 104 barrier traps. D) Two examples of microfluidic traps in which a switching event occurred. The strain contains the Wor1-GFP fusion protein and cells enter the trap (from the right) as white cells. As cells complete switching to the opaque state, the Wor1-GFP fusion reaches high levels of expression.

VIDEO 1 legend – Example of time-lapse movie of a switching event
Movie corresponds to 'Example 1' in FIGURE 1D. Movie is shown twice; in the second repetition, tracked cells are labeled. This strain contains the Wor1-GFP fusion protein.

Observations on pseudohyphal growth and mitosis

Consistent with a previous report (Bergen et al., 1990), we observed elongated cells reminiscent of pseudohyphae (Sudbery et al., 2004) as intermediates in some instances of white-opaque switching. Typically a round mother cell buds an elongated cell and both subsequently activate Wor1 (FIGURE 2, FIGURE S2). It is possible that pseudohyphal formation increases the probability of switching; however, it is not necessary or sufficient for switching as we observed pseudohyphal formation without switching and switching without pseudohyphal formation. In the majority of cases, descendents of initial

213 switching cells resemble typical opaque cells (which are slightly more elongated than
214 white cells) within a few cell divisions.
215

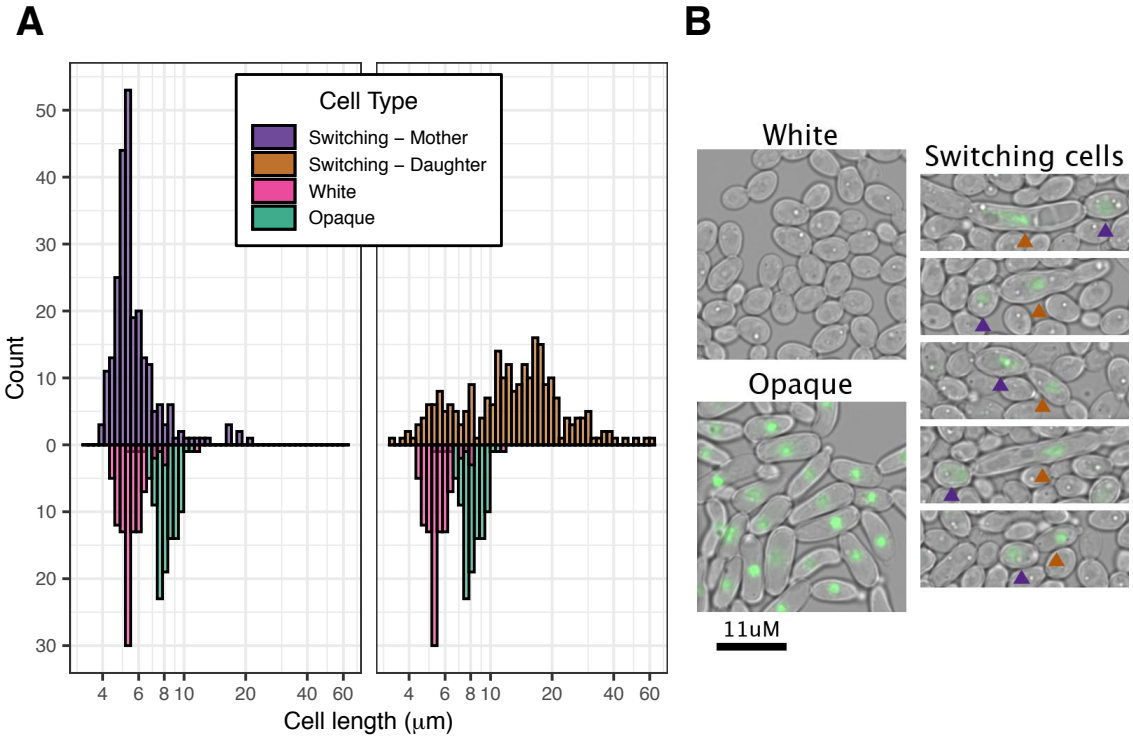

216
217
218 FIGURE 2 legend – Cell length distribution of switching cells
219 A) Cell length distribution of switching cells compared to typical white and opaque cells.
220 Switching initiates in pairs of mother and daughter cells, the left histogram shows the size
221 distribution for mothers, the right, for daughters. Typical white and opaque cell
222 distributions are shown beneath each histogram for reference. The strain contains the
223 Wor1-GFP fusion protein. X-axis is logarithmic B) Representative images of white,
224 opaque and cells undergoing white to opaque switching. Arrows point out mother and
225 daughter in each switching pair with colors corresponding to (A). Although elongated
226 (pseudohyphal) cells are observed, they are neither necessary nor sufficient for switching.
227
228 Although not a primary goal of this work, the nuclear localization of Wor1 allowed us to
229 observe certain features of mitosis in switching cells. In a subset of cases, nuclear
230 division occurred within the elongated daughter cell and not across the bud neck
231 (FIGURE S3). Similar observations have been seen in filamentous forms of *C. albicans*
232 (Sudbery et al., 2004). In some of our examples, one of the two nuclei in the daughter cell
233 returned to the mother cell and both cells continued dividing (FIGURE S3A). In other
234 examples, both nuclei remained in the elongated daughter forming polyploid cells
235 (FIGURE S3B). In these cases, the mother cell no longer divided. This distinctive mitosis
236 pattern did not always occur during switching and, as a result, the majority of opaque
237 cells are not polyploid. Although we were able to observe these deviations from
238 conventional mitosis, they are not required for switching, as we did not observe them in

239 all switching events. Furthermore, these atypical mitosis events are likely specific to *C.*
240 *albicans* cells and do not represent a general feature.
241
242 *WOR1 activation is synchronous in mother-daughter pairs and is stereotypical across*
243 *independent switching events*
244
245 To quantify switching, we developed a custom semi-automated image analysis pipeline to
246 measure Wor1-GFP (or Wor1-mGFP) levels in single cells over time (FIGURE S4,
247 METHODS). Because Wor1 is nuclear localized, we used the average of the 300 highest
248 intensity pixels per cell as a quantitative measure of Wor1 levels. During switching,
249 Wor1 levels increase and then oscillate in concert with nuclear divisions similar to those
250 observed in established opaque cells (FIGURE 3A). Comparing Wor1 activation in
251 mother cells of independent switching events (taken from different traps and
252 experiments) reveals a generally stereotypical response (FIGURE 3B) taking
253 approximately three hours to reach maximum Wor1 levels. Consistent with the stochastic
254 nature of switching, the starting time of different switching events did not depend on the
255 time (or number of cell divisions) from the beginning of the experiment. Moreover, even
256 the time between the birth of a switching cell and its switching varies from one cell to the
257 next.
258
259 As mentioned above, Wor1 activation occurs in dividing cells where both mother and
260 daughter cells typically activate Wor1 simultaneously. This synchronous activation at
261 times extends to the mother cells' previous daughter as well, leading to four cells
262 (mother, two daughters and one granddaughter) activating Wor1 simultaneously
263 (FIGURE 3C, 3D). The synchrony in Wor1 activation between mother and daughter cells
264 suggest the pace of Wor1 activation is determined early in the switching event. Once high
265 levels of Wor1 were reached, they were always inherited across subsequent cell divisions
266 indicating that the switch was complete.

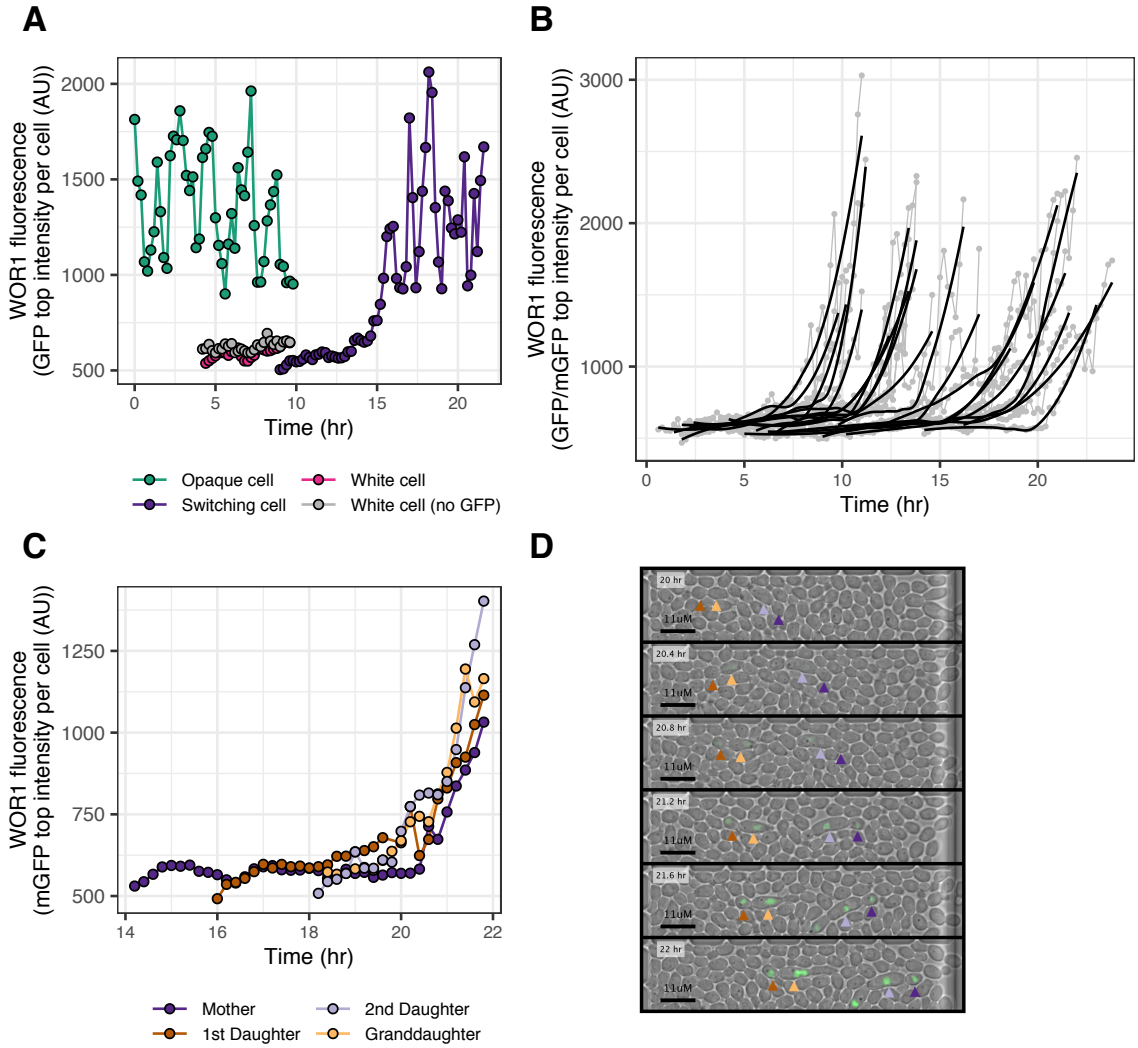

FIGURE 3 legend – Wor1 fluorescence (GFP/mGFP) levels in single cells
A) Representative example of a Wor1 expression level trace in a single switching cell (purple). Traces of typical white (pink) and opaque (green) cells are shown for reference. Oscillations in high Wor1 levels occur with nuclear divisions. X-axis represents time from the beginning of the experiment; examples are taken from cells born at different times. The strain contains the Wor1-GFP fusion protein. B) Examples of Wor1 activation in single switching cells. Traces (grey points and lines) are truncated to highlight the initial activation of Wor1. Black lines represent locally estimated scatter-plot smoothing (LOESS) of individual traces. Examples are taken from three different experiments, representing strains containing the Wor1-GFP (n=17) or the Wor1-mGFP (n=4) fusion protein. C) Representative example of a four-cell (direct mother-daughter) pattern of synchronous Wor1 activation. X-axis represents time from the beginning of the experiment and traces are shown starting at the birth of the mother cell. The strain contains the Wor1-mGFP fusion protein. D) Subset of images representing data shown in (C) with time proceeding from top to bottom. Arrows point to individual cells with colors corresponding to (C). All four switching cells simultaneously activate Wor1.

286 *Certain lineages of cells show unusual switching patterns*
287
288 An unanticipated feature of white-opaque switching emerged when we reconstructed
289 complex pedigrees of switching cells, tracing the prior histories of cells destined to
290 switch. In addition to the simple pairs of mother-daughter cells activating Wor1
291 simultaneously described above, we observed instances where additional cells in the
292 same trap also activated Wor1. Pedigree analysis revealed that these additional cells were
293 closely related to the conventional mother-daughter switching pairs, through a previous
294 mother, daughter or sister (FIGURE 4A). However, these related switching cells were
295 separated by cell divisions that produced cells that did not switch, creating small mixed-
296 fate pedigrees (FIGURE4A).
297
298 To determine if these cases are the result of entirely independent switching events or are
299 due to a complex pattern of switching within a single linage, we analyzed the Wor1-
300 mGFP strain, where overall switching rates are lower. We estimate the Poisson
301 probability distribution for multiple switching events per trap based on the proportion of
302 traps where there was no Wor1 activation (134/168 traps) (FIGURE 4B, METHODS).
303 We find that the Poisson expectation (FIGURE 4B, white bars) of switching events is
304 matched exactly when considering direct mother-daughter and mixed-fate pedigrees as
305 single dependent switching events (Chi-squared goodness of fit p-value, 0.986),
306 (FIGURE 4B, light grey bars). However, the expectation is not matched if direct mother-
307 daughter pedigrees are considered dependent but mixed-fate pedigrees are considered two
308 independent events (Chi-squared goodness of fit p-value, 0.0034), (FIGURE 4B, medium
309 grey bars). This analysis rules out multiple independent events as the explanation for
310 mixed-fate pedigrees and indicates that the switching events must be related to each
311 other.
312
313 One common pattern of mixed-fate pedigree involved a mother cell budding three cells in
314 succession (top-right "Mixed fate" pattern shown in FIGURE 4A). While the mother and
315 the first and the third daughters ultimately activate Wor1, the second daughter does not
316 (FIGURE 4C, 4D, VIDEO 2). With the Wor1-GFP fusion protein, we also observe
317 similar patterns, including an example where a subset of the decedents of the second
318 daughter also activates Wor1 (FIGURE S5). These observations suggest that certain cells
319 undergo a stochastic event that predisposes them and their direct descendents to a higher
320 probability of switching then that observed in the general population. Whether or not
321 cells in these pedigrees actually undergo switching appears to be determined by a second
322 event. We do not know the basis of the first event (see discussion), but in the next
323 sections, we further explore the second step in which certain cells rapidly increase Wor1
324 expression.

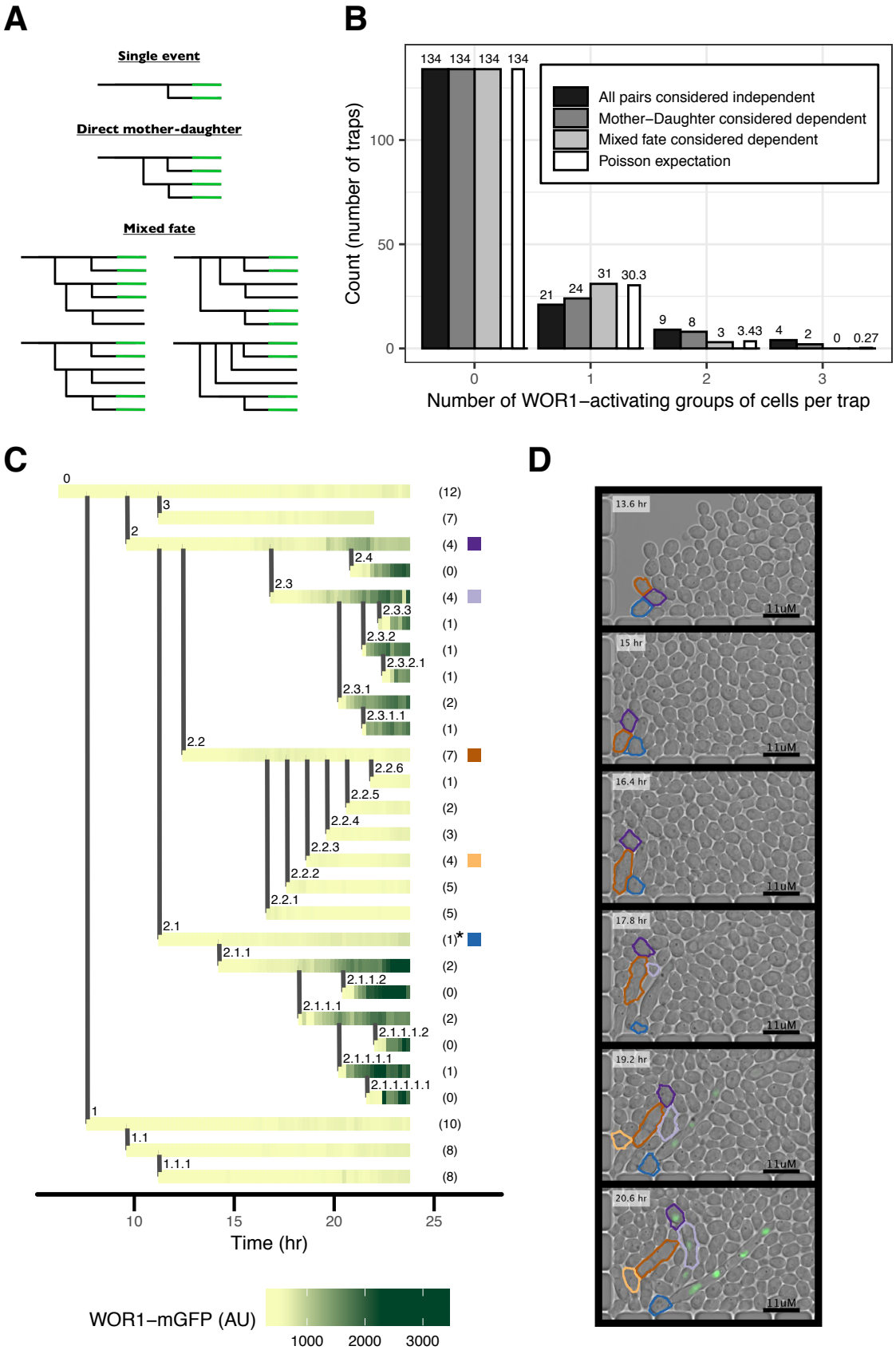
A
Single event
Direct mother-daughter
Mixed fate
B
Count (number of traps)
Number of WOR1−activating groups of cells per trap
All pairs considered independent
Mother−Daughter considered dependent
Mixed fate considered dependent
Poisson expectation
134 134 134 134
21 24 31 30.3
9 8 3 3.43 4 2 0 0.27
C
Time (hr)
WOR1−mGFP (AU)
1000 2000 3000
D
13.6 hr
15 hr
16.4 hr
17.8 hr
19.2 hr
20.6 hr
11uM

326 FIGURE 4 legend – Wor1 activation in pedigrees
327 A) Schematic of pedigree patterns of Wor1 activation, including several examples of
328 mixed-fate pedigrees. Horizontal lines represent single cells; vertical lines represent
329 budding of a daughter cell. Green color represents Wor1 activation. B) Comparison of
330 distributions of the number of switching events per trap to Poisson expectation (white
331 bars). Different distributions are based on including different classes of pedigree patterns
332 as single dependent events. The strain contains the Wor1-mGFP fusion protein. C)
333 Representative mixed-fate pedigree (top-right "Mixed fate" pattern shown in (A)).
334 Horizontal lines represent single cells; vertical lines represent budding of a daughter cell.
335 Every horizontal line is made up of small tiles representing the measured Wor1-mGFP
336 fluorescence at that time. Numbers within parentheses on the right of the pedigree
337 represent the number of budded daughter cells per cell within the time period shown; not
338 all daughters are depicted in the pedigree. The cell marked by the asterisk lost its nucleus
339 to its daughter cell. Colored square tiles on the right-hand side indicate individual cells
340 that are depicted in (D) using the same color scheme. D) Subset of images representing
341 data shown in (C) with time proceeding from top to bottom. Cell outlines are based on
342 automated image analysis (METHODS).
343
344 VIDEO 2 legend – Example of time-lapse movie of a switching event containing a
345 mixed-fate pedigree
346 Movie corresponds to example in FIGURE 4C. Movie is shown twice; in the second
347 repetition, tracked cells are labeled. This strain contains the Wor1-mGFP fusion protein.
348
349 *Using a synthetic inducible system in Saccharomyces cerevisiae to investigate the*
350 *properties of Wor1 autoregulation*
351
352 Wor1 has been shown to bind to its own control region and to activate its own expression
353 (Zordan et al., 2006). This positive feedback loop has been proposed to be a critical
354 feature of white-opaque switching. Consistent with this hypothesis, we found that the
355 frequency of white-opaque switching is reduced when a single Wor1 motif (out of nine)
356 from the Wor1 control region is deleted (TABLE S1, METHODS). In addition to Wor1,
357 at least 7 other regulators bind the Wor1 control region (Hernday et al., 2013; Lohse &
358 Johnson, 2016), which complicates studying Wor1 autoregulation directly in *C. albicans*.
359 To study Wor1 autoregulation without these confounding factors, we set up the Wor1
360 autoregulatory loop using a synthetic biology approach (Aranda-Díaz et al., 2017;
361 McIsaac et al., 2014). Specifically, we developed a system in *S. cerevisiae* where we can
362 induce the expression of the *C. albicans* Wor1 protein with progesterone (METHODS,
363 FIGURE 5A) and use flow cytometry to follow the activation of Wor1 transcription using
364 a florescent reporter driven by the *C. albicans* Wor1 regulatory region (METHODS).
365
366 The 7KB control region (enhancer) of the *C. albicans* Wor1 was fused to the *S.*
367 *cerevisiae* Cyc1 core promoter (METHODS) resulting in a reporter that was specifically
368 activated by Wor1 expression (FIGURE S6). Using an mCherry fluorophore for the
369 transcriptional reporter, we created independent (a or α mating type) strains where levels
370 of Wor1, Wor1-GFP, Wor1-mGFP or GFP could be controlled from a synthetic
371 expression construct by adding hormone (METHODS). Comparing Wor1-GFP to Wor1-

372 mGFP is informative as the ability of GFP to dimerize is the basis for increased switching
373 in *C. albicans* with Wor1-GFP (TABLE S1). All GFP and mCherry measurements were
374 normalized by forward scatter (METHODS). As expected, GFP, Wor1-GFP and Wor1-
375 mGFP fluorescence all increased in a hormone dependent manner when driven by the
376 synthetic hormone dependent construct (FIGURE 5B left, FIGURE S7A). Despite
377 identical transcriptional constructs, GFP was induced at ten fold higher levels than Wor1-
378 GFP and Wor1-mGFP (FIGURE 5B left), possibly due to differences in mRNA or
379 protein stability or to translational efficiency. Inducing Wor1 or its GFP fusions also
380 caused physiological effects such as cell clumping, leading to increased autofluorescence
381 (in the Wor1 strains) and bimodal induction distributions (in the Wor1-GFP strains). *S.*
382 *cerevisiae* has two Wor1 homologs (*MIT1* and *ROF1*) with conserved DNA binding
383 domains and motifs. We created strains where both homologs are deleted and found that
384 the results did not change significantly. We present data for both sets of strains.
385
386 *Wor1 autoregulation is ultrasensitive and the effect of GFP dimerization informs*
387 *potential mechanism for increasing switching frequency*
388
389 The Wor1 transcriptional reporter shows low levels of expression in the absence of
390 hormone (FIGURE S7B). As hormone levels increase, the reporter is activated in strains
391 where the hormone induces Wor1 or its GFP fusions but not when GFP alone is produced
392 (FIGURE5B right). In strains inducing Wor1-GFP and Wor1-mGFP, we could measure
393 both the level of the fusion protein (via the GFP channel) and the response of the Wor1
394 enhancer (via the mCherry channel) in single cells (FIGURE 5C, FIGURE S8A). To
395 quantify the response function of Wor1 autoregulation, we fit four-parameter log-logistic
396 functions (Hill equations) that describe S-shaped curves, to these distributions using
397 least-squares estimation (METHODS, FIGURE 5C, 5D). The four parameters specify the
398 lower horizontal asymptote, the upper horizontal asymptote, the value at which the
399 response is half of the maximum and the Hill coefficient, which is a measure of the
400 steepness of the response curve (ultrasensitivity). Hill coefficients greater than 1 imply
401 cooperativity in gene regulation. As reporter expression gradually decreases at high
402 hormone levels in strains containing Wor1-GFP, we only used a subset of conditions for
403 fitting in these strains (METHODS, FIGURE S8A). The decrease under these conditions
404 suggests high levels of Wor1 dimers might negatively regulate Wor1 expression. All
405 curves were ultrasensitive (FIGURE 5D) with mean Hill coefficient estimates of 3.2
406 (standard deviation, 0.4) for Wor1-mGFP and 4.3 (standard deviation, 0.9) for Wor1-
407 GFP. While there was a small but significant increase in cooperativity for Wor1-GFP
408 over that of Wor1-mGFP (t.test p.value, 0.01), there was a striking difference in the level
409 of protein required for half-max activation, with 5 times higher levels required for Wor1-
410 mGFP than Wor1-GFP (t.test p.value, 8.04e-05). As the ability of GFP to dimerize most
411 likely increases the effective amount of Wor1 found in dimers, the difference in
412 activation thresholds suggests that Wor1 normally acts as a multimer to efficiently bind
413 DNA. Wor1-GFP levels in *C. albicans* opaque cells are comparable to the levels of
414 Wor1-GFP needed to activate the reporter in our synthetic *S. cerevisiae* system (FIGURE
415 S8B), further indicating that the synthetic system captures features of the authentic *C.*
416 *albicans* circuit.

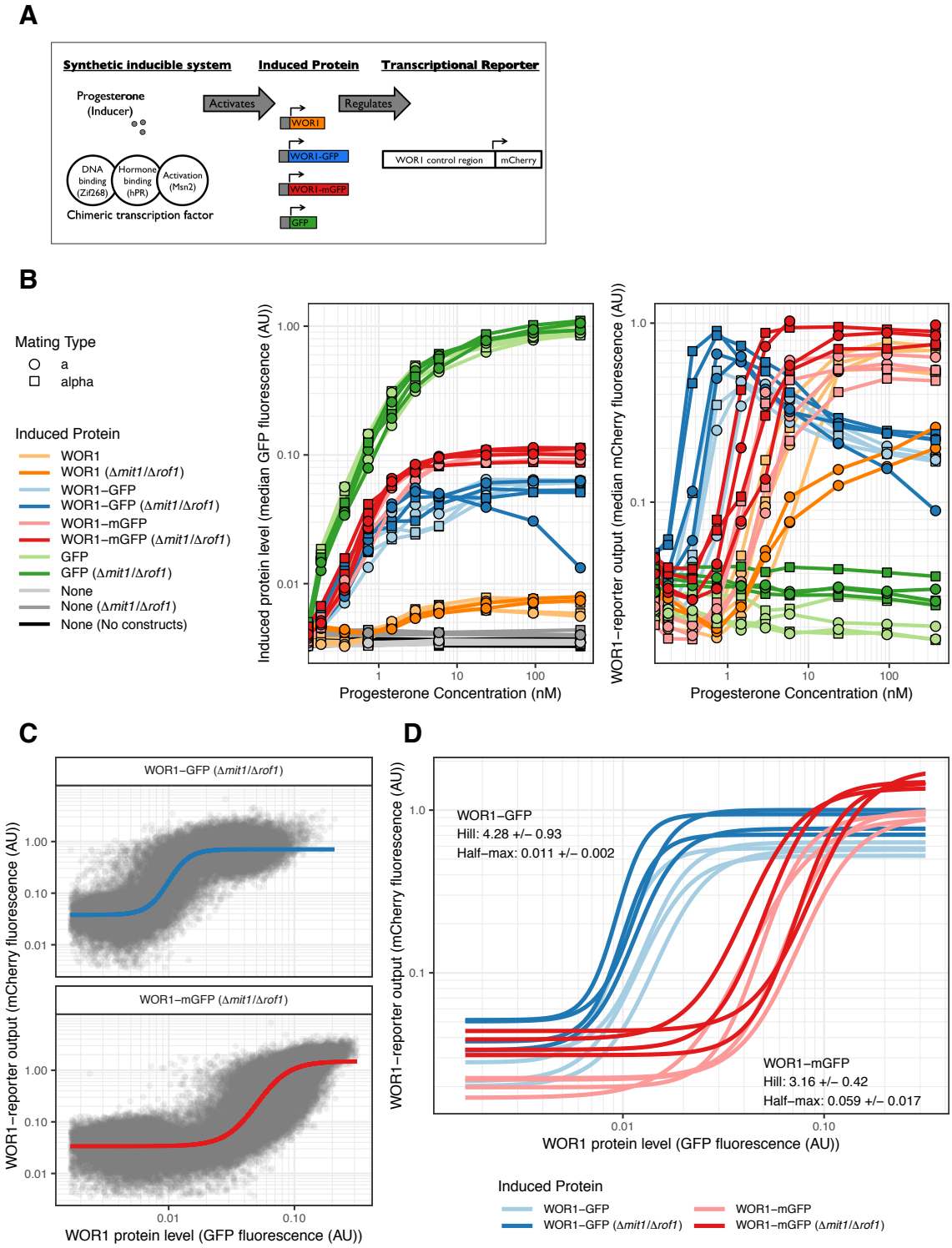
A
Synthetic inducible system
Induced Protein
Transcriptional Reporter
Progesterone (Inducer)
Activates
Regulates
WOR1
WOR1-GFP
WOR1-mGFP
GFP
WOR1 control region
mCherry
DNA binding (Zif268)
Hormone binding (hPR)
Activation (Msn2)
Chimeric transcription factor
B
Mating Type
a
alpha
Induced Protein
WOR1
WOR1 (Δmit1/Δrof1)
WOR1–GFP
WOR1–GFP (Δmit1/Δrof1)
WOR1–mGFP
WOR1–mGFP (Δmit1/Δrof1)
GFP
GFP (Δmit1/Δrof1)
None
None (Δmit1/Δrof1)
None (No constructs)
Induced protein level (median GFP fluorescence (AU))
WOR1–reporter output (median mCherry fluorescence (AU))
Progesterone Concentration (nM)
C
WOR1–GFP (Δmit1/Δrof1)
WOR1–mGFP (Δmit1/Δrof1)
WOR1–reporter output (mCherry fluorescence (AU))
WOR1 protein level (GFP fluorescence (AU))
D
WOR1–GFP
Hill: 4.28 +/– 0.93
Half–max: 0.011 +/– 0.002
WOR1–mGFP
Hill: 3.16 +/– 0.42
Half–max: 0.059 +/– 0.017
WOR1–reporter output (mCherry fluorescence (AU))
WOR1 protein level (GFP fluorescence (AU))
Induced Protein
WOR1–GFP
WOR1–GFP (Δmit1/Δrof1)
WOR1–mGFP
WOR1–mGFP (Δmit1/Δrof1)

422 FIGURE 5 legend – Wor1 autoregulation parameters determined by a synthetic inducible
423 system in *Saccharomyces cerevisiae*
424 A) Schematic of experimental design. B) Median GFP (left) or mCherry (right)
425 fluorescence for strains inducing different proteins in a range of hormone concentrations.
426 Every set of constructs is represented by four independently constructed strains, each
427 measured on two different days (with the exception of the Wor1 (Δ*mit1*/Δ*rof1*) strains
428 which were only measured once). X-axis and Y-axis are logarithmic. C) GFP (Wor1
429 protein) and mCherry (Wor1 transcriptional activity) fluorescence for individual cells
430 across hormone concentrations. Data is shown for two strains inducing either Wor1-GFP
431 (top) or Wor1-mGFP (bottom) measured on one day. Solid line represents fit Hill
432 equation for each strain. X-axis and Y-axis are logarithmic. D) Fit Hill equation curves
433 for Wor1 transcription activity of strains inducing either Wor1-GFP (blue) or Wor1-
434 mGFP (red). Each curve is fit to data measured on one of two different days. Inset text
435 summarizes parameters for each set of strains (mean +/- standard deviation). X-axis and
436 Y-axis are logarithmic.
437
438
439

Discussion

The ability of cells to switch between different cellular states, each of which are faithfully inherited through many rounds of cell division, underlie a wide range of important phenomena including cell differentiation (Sánchez Alvarado & Yamanaka, 2014), antibiotic resistance (Kussell, 2005a; Van den Bergh et al., 2017) and cancer progression (Rosen & Jordan, 2009). The fungal pathogen *Candida albicans* and its close relatives *Candida dubliniensis* and *Candida tropicalis* all undergo a phenomenon known as white-opaque switching, whereby two distinct states are stable across many cell divisions, and switching between them is stochastic (Porman et al., 2011; Pujol et al., 2004). Although the presence of these heritable states has been preserved by selection in these species, the mechanism of switching and the complete range of physiological roles of the two cell types are topics of active investigation. It is known that opaque cells are the mating competent cell type (Miller & Johnson, 2002) and are less susceptible to phagocytosis by macrophages, potentially promoting immune evasion (Lohse & Johnson, 2008; Sasse et al., 2013). Recent work has also shown that, due to a specialized secreted protease program, a small number of opaque cells can promote growth of a large white cell population; thus the two cell types can act synergistically (Lohse et al., 2020). Aside from its physiological roles, white-opaque switching has many advantages as a eukaryotic system to study stochastic phenotypic switching. It exemplifies two crucial phenomena, rare stochastic phenotypic switching and cell states that are stable through thousands of cell divisions. It shares many features with similar networks in multicellular eukaryotes, such as a large number of transcription factors and long, complex regulatory regions (enhancers). White-opaque regulators have also been shown to form phase-separated condensates (Frazer et al., 2020), which are a feature of some mammalian enhancers (Boija et al., 2018). A particular advantage of studying phenotypic switching and heritability in *C. albicans* is the relative ease of performing genetic manipulations. By combining genetic modifications with direct observation of single cells, our goal is to describe in quantitative terms the molecular mechanisms that underlie cell type switching.

Positive feedback, encompassing either positive interactions, double negative interactions, or autocatalysis is necessary, but not sufficient for the creation of heritable cell states (Ferrell, 2002). To facilitate switching, the response must incorporate non-linearity, also known as ultrasensitivity, in order to create sharp transitions from gradual changes (Ferrell & Ha, 2014). Mechanisms for creating or increasing ultrasensitivity in regulatory responses include cooperative binding of transcriptional regulators (Ackers et al., 1982; Burz, 1998; Johnson et al., 1981), protein sequestration of regulators (Buchler & Cross, 2009) and the number of steps in transcriptional cascades (Hooshangi et al., 2005). We show here that Wor1 regulation of its own promoter is ultrasensitive even in the absence of other *C. albicans* regulators. While difficult to test in the native *C. albicans* system, we propose this ultrasensitive response is a crucial feature of white-opaque switching which can be incorporated into mathematical models describing switching (Sriram et al., 2009). Furthermore, the propensity to dimerize added by the GFP causes a small increase in the steepness of the activation curve but a large reduction in the activation threshold. It is this large reduction in activation threshold that likely

485 leads to the large increase in white-opaque switching in *C. albicans* cells that harbor
486 Wor1-GFP. This observation suggests switching depends on the equilibrium between
487 Wor1 monomers and higher oligomers. While the natural threshold results in rare
488 switching under standard lab conditions, our results show that switching frequency is
489 easily adjusted by a relatively small change in the propensity of Wor1 to dimerize.
490 Indeed, other white-opaque regulators may function in a similar manner to the GFP
491 fusion; any increase in Wor1 multimer formation would produce a large effect on
492 switching and could amplify a small amount of Wor1 expression. Although many
493 questions remain concerning the molecular details of Wor1 autoregulation, our results
494 quantify, for the first time, the ultrasensitivity of the WOR1 control region (enhancer) in
495 response to carefully measured levels of the Wor1 protein.
496
497 A particular advantage of our study is the use of microfluidics, which has allowed us to
498 observe white-opaque switching at a single cell level and at high temporal resolution. The
499 ability to track single cells and their lineages through time allowed us to make an
500 unexpected observation, that switching can occur in multiple groups of related cells, even
501 when these groups are separated by cell divisions that produce cells that do not switch.
502 The presence of this pattern did not differ between strains containing Wor1-GFP versus
503 Wor1-mGFP despite different switching frequencies. We can draw two conclusions from
504 this switching pattern. First, at least two stochastic events are needed for cells to switch
505 from white to opaque. The first event defines small pedigrees of cells with increased
506 probability of switching and the second event, which only occurs in a subset of cells in
507 these pedigrees, directly leads to Wor1 activation and cell switching. Second, when a
508 complete switching event occurs, several closely related cells in the pedigree switch
509 simultaneously, a property that may be adaptive. The occurrence of coordinated
510 switching would be advantageous in situations where the rapid generation of the rare cell
511 type could be beneficial. For *C. albicans*, increasing the number of opaque cells could be
512 valuable both for immune evasion or metabolic cooperation with white cells. A similar
513 switching pattern was observed in a lab-modified galactose utilization pathway in
514 *Saccharomyces cerevisiae* (Kaufmann et al., 2007). In that study, removal of negative
515 feedback created a system dominated by a single positive feedback loop and led to cells
516 stochastically turning on the GAL regulon in the absence of galactose. In a very similar
517 manner to our observations, the authors saw correlated activation in cell pedigrees, at
518 times separated by cells not activating GAL expression (Kaufmann et al., 2007). This
519 comparison suggests these coordinated switching patterns might be a general feature in
520 eukaryotic systems.
521
522 One hypothesis to account for our observed correlations among related cells relies on the
523 stochastic and bursty nature of gene expression (Raj & van Oudenaarden, 2008).
524 According to this hypothesis, the first stochastic event during white-opaque switching
525 might be a rare burst of low-level Wor1 transcription in the absence of efficient
526 translation of Wor1 mRNA. Because no Wor1 is made, this state would be heritable over
527 only a small number of cell divisions, defining the small pedigrees of cells predisposed to
528 switch. The second stochastic event could then depend on variation in translation
529 efficiency (or uneven partitioning during division), with only certain cells in the pedigree
530 accumulating sufficient Wor1 protein to excite the Wor1 positive feedback loop, leading

to high level Wor1 expression and subsequent cell-type switching. Consistent with this hypothesis, the Wor1 UTR severely reduces Wor1 protein expression (Guan & Liu, 2015). This hypothesis is subject to explicit testing and will be the focus of future work.

Our work has resolved several issues needed for a quantitative molecular understanding of white-opaque switching and lays the foundation for subsequent hypothesis tests. While white-opaque switching and the genetic network that controls it are highly complex, it represents one of only a few cases of a true epigenetic change in a eukaryotic cell that does not require external signals and is simple enough to be analyzed in detail and ultimately, understood in great depth.

542 Materials and methods
543
544 ***C. albicans* strain construction**
545 The genetic background for *C. albicans* is SC5314. SNY425 was used as a prototrophic
546 a/α reference strain (Noble et al., 2010). For a prototrophic a/Δ reference strain, the α
547 copy of the MTL in SNY250 (Noble & Johnson, 2005) was replaced with a copy of
548 *ARG4* using pJD1 (Lin et al., 2013). Genetic modifications were created using a *SAT1*
549 marker-based CRISPR protocol targeting *Candida maltosa LEU2* (Nguyen et al., 2017).
550 Homozygous Wor1-GFP and Wor1-mGFP fusion proteins were created at the
551 endogenous *WOR1* locus using a combination of two guides encompassing the stop
552 codon (GGTACTTAGTTGAATTAATA and GTACTTAGTTGAATTAATAC). Donor
553 DNA was created by restricting plasmids containing the GFP (or mGFP) sequence
554 flanked by 500 bp of homology to the 3' end of the *WOR1* ORF and 3' UTR (Lohse &
555 Johnson, 2010). The *WOR1* motif deleted from the *WOR1* promoter consists of three
556 overlapping binding motifs (17bp, AAAGTTTAAACTTTAAA), found 5802 bp
557 upstream of the translation start site. A combination of two guides were used for creating
558 the deletion (GAAATTTATGAAAGACGGGT and ACCAGTAGTGATTCATAAAT),
559 donor DNA consisted of 90 bp oligos containing 45 bp homology to flanking sequences
560 with two single bp substitutions to disrupt PAM or guide sequences
561 (AATAATTAGAGTTTTACAAGAAATTTATGAAAGACGGGTGcGAAATACTATA
562 AAATAGAGCAATAAATGACAGAACCTAgCAGTAGTGAT).
563
564 ***S. cerevisiae* strain construction**
565 The genetic background for *S. cerevisiae* experiments is S288C. Starting strains were
566 mating type a or α with multiple auxotrophies, created by mating FY23 (*leu2Δ1 ura3-52*
567 *trp1Δ63*) (Winston et al., 1995) and a mating type α spore of BY4743 (*his3Δ1 leu2Δ0*
568 *lys2Δ0 met15Δ0 ura3Δ0*) (Brachmann et al., 1998). Subsequent transformations
569 integrated various constructs in the following order: the chimeric transcription factor,
570 deletion of the *WOR1* homologs, the induced protein (GFP, Wor1-GFP, Wor1-mGFP or
571 Wor1) and the *WOR1* transcriptional reporter. Plasmids were constructed using either
572 restriction digest and subsequent ligation or by using homology based cloning (In-Fusion,
573 Takara 638911) and were sequence verified, all PCRs utilized a high fidelity polymerase
574 (CloneAmp HiFi PCR Premix, Takara 639298). Plasmids contained components of the
575 synthetic inducible system flanked by homology to the intended genomic integration
576 locus and were restricted prior to transformation. The chimeric transcription factor used
577 is "Z3PM" (Aranda-Díaz et al., 2017) which consists of the Zif268 DNA binding domain,
578 hPR ligand binding domain and the yeast Msn2 activation domain. The transcription
579 factor was expressed from the *S. cerevisiae ADH1* promoter and terminated by the *C.*
580 *albicans ADH1* terminator. The transcription factor was integrated into *leu2* proceeded by
581 the *Candida glabrata LEU2* sequence, including promoter and terminator. Induced
582 proteins were expressed from a modified *GAL1* promoter containing three dimeric Zif268
583 binding sites (Aranda-Díaz et al., 2017) and terminated by the *C. albicans ADH1*
584 terminator. The proteins were integrated into the *trp1* locus proceeded by the *C. glabrata*
585 *TRP1* sequence, including promoter and terminator. The *WOR1* homologs (*MIT1* and
586 *ROF1*) were knocked out using a plasmid based CRISPR approach (Ryan et al., 2014). A
587 plasmid with a 2μ origin of replication was constructed that contained Cas9, a KanMX

588 selection cassette and two guides (one for each of the homologs). The guides were
589 expressed from the *SNR52* and *SUP4* promoters respectively and both were terminated by
590 a copy of the *SNR52* terminator. Donor DNA consisted of 90bp complementary annealed
591 oligos (Nguyen et al., 2017) containing 44 bp of homology upstream and downstream of
592 the ORF, flanking a GG sequence. After verifying both homologs were deleted, cells
593 were grown overnight in the absence of G418, plated on YPD and replica plated to
594 YPD+G418 to identify colonies that had lost the *CAS9* containing plasmid. The main
595 *WOR1* transcriptional reporter consists of 6656 bp of the *WOR1* promoter (ending at a
596 presumed TATA box, 2048 bp before the translational start site), 115 bp containing the
597 end of the *CYC1* promoter and it's 5' UTR (starting at the "-52" TATA box (Hahn et al.,
598 1985)) and a fluorescent protein ORF (mCherry or GFP) followed by the *C. albicans*
599 *ACT1* terminator. An alternative reporter contained an additional 70 bp of the end of the
600 *WOR1* promoter and 1980 bp encompassing the *WOR1* 5'UTR instead of the *CYC1*
601 sequence. Transcriptional reporters were preceded by a Hygromycin resistance cassette
602 and integrated into the *ura3* locus. Integration was achieved using two separate restricted
603 plasmids simultaneously transformed. One plasmid contained homology upstream to the
604 *URA3* locus, the Hygromycin cassette and the *WOR1* promoter and beginning of 5' UTR.
605 The second plasmid contained the end of the *WOR1* promoter, the *CYC1* (or *WOR1*)
606 5'UTR, the florescent protein and terminator and homology downstream to the *URA3*
607 locus. With one exception, combinations of constructs were represented by two
608 completely independent strains based on different starting strains (of mating type a or α).
609 The induced Wor1 (Δ*mit1*/Δ*rof1*) combination was represented by two mating type a
610 strains.
611
612 **Microscopy and microfluidics**
613 *C. albicans* strains were streaked from frozen stocks on SD+aa+uri plates and incubated
614 for 5-9 days at 25°C. Colonies were directly diluted to an OD of 0.25 and grown in liquid
615 SD+aa+uri for 4 hours. Cultures were washed and diluted to approximately $5X10^6$
616 cells/ml in PBS without calcium or magnesium and 50ul were loaded into microfluidic
617 plates. For microfluidic experiments, we used a CellASIC® ONIX microfluidic platform
618 and corresponding Y04T-04 plates. Each plate contains four separate chambers, each
619 chamber containing 104 individual traps. Images were captured using a Nikon Ti2-E
620 microscope equipped with a Photometrics Prime 95B-25mm Camera and a CFI60 Plan
621 Apochromat Lambda 100x Oil immersion objective lens. Cells were loaded into the plate
622 chambers using 55.1 kPa of pressure for 5 seconds and media (SD+aa+uri) flow was
623 started immediately. The media flow program consisted of cycles of three 5 second bursts
624 of perfusion at 10 kPa from each of six inlet channels followed by an hour of perfusion at
625 1.7 kPa from each of six inlet channels. Coordinates for fields containing single traps
626 loaded with at least one cell were manually determined. Nikon NIS Elements software
627 was used to drive stage movement and acquisition; the Nikon Perfect Focus System was
628 utilized. Images (DIC and GFP channels) were captured for each field (40-70 per
629 chamber) every 12 minutes for 24 hours. Temperature was kept at 25°C using an
630 OKOLab Cage Incubator.
631
632
633

634 **Image and data analysis**
635 Custom Matlab scripts were used for image analysis; statistical analysis and data
636 visualization utilized R (R Core Team, 2019), with extensive use of *tidyverse* (Wickham,
637 2017). Images were first adjusted to correct for stage movement. Each image was
638 compared to the previous image in the time series and the optimal geometric
639 transformation was found to account for any (x,y) movement (Matlab function
640 *imregtform*). Next, cells were segmented automatically in each image. Cell borders were
641 identified using a combination of bottom hat filtering, top hat filtering, dilation, erosion
642 and selection based on object properties (area, perimeter and eccentricity). Individual
643 cells were tracked through time by manually determining their position in a series of
644 images; each position was then associated with the corresponding automatically
645 segmented cell. Pedigree information was also manually determined. For a metric of
646 Wor1 expression per cell, the 300 highest intensity pixels (in the GFP channel) were
647 averaged. Typical white cell size is 1,750 pixels; typical opaque cell size is 2,500 pixels.
648 Cell length (FIGURE 2, FIGURE S2) was determined using Fiji (Schindelin et al., 2012)
649 by recording the length of a line drawn along the cells long axis. Cell length was recorded
650 when cells were beginning to bud a new cell. 100 reference white and opaque cells were
651 recorded. Cell length was recorded for all pairs of switching cells across three
652 experiments from different days, resulting in 248 mother-daughter pairs of cells
653 containing Wor1-GFP and 50 pairs of cells containing Wor1-mGFP. For determining if
654 mixed-fate pedigrees represent two independent switching events, we considered 168
655 traps loaded with cells containing Wor1-mGFP. The numbers of switching events were
656 counted in each trap according to three different ways of calculating independent events:
657 1) every pair of mother-daughter cells are considered independent, 2) pairs of direct
658 mother-daughter pairs are no longer considered independent, 3) pairs in mixed-fate
659 pedigrees are also no longer considered independent. We calculated the expected Poisson
660 probability distribution based on the unambiguous zero-class of 134 traps (λ=-
661 log(134/168)). We performed chi-squared goodness-of-fit tests with p-values computed
662 by Monte Carlo simulations with 2000 replicates.
663
664 **Flow cytometry, experiments and data analysis**
665 *S. cerevisiae* strains were streaked from frozen stocks on YPD plates and incubated for 2
666 days at 30°C. Colonies were inoculated into 3ml of SD+aa+uri media and grown
667 overnight. Cells were washed, resuspended in PBS without calcium or magnesium and
668 diluted 1:16 into 96-well plates containing SD+aa+uri with different concentrations of
669 progesterone. Progesterone was diluted from 2mM stocks (95% Ethanol, 5% DMSO);
670 lower concentrations were supplemented with Ethanol and DMSO to match the high
671 concentration. Plates contained 8 experimental strains measured at 10 different
672 concentrations of progesterone and 3 control strains measured at 4 concentrations of
673 progesterone. For each set of strains two identical plates were created and incubated,
674 shaking at 500 RPM at 30°C. After a set incubation time, plates were washed three times
675 and diluted in PBS without calcium or magnesium with 1mM EDTA. One plate was read
676 after 4.5 hours of incubation and the second was read at 24 hours. Data from both plates
677 were similar and the 24-hour readings are presented. Measurements were taken using a
678 BD FACSCelesta. GFP fluorescence was measured by blue (488nm) excitation and a
679 530/30 band pass emission filter. mCherry fluorescence was measured by yellow-green

680 (561nm) excitation and a 610/20 band pass emission filter. Flow cytometery data was
681 analyzed using R (R Core Team, 2019), with extensive use of *tidyverse* (Wickham,
682 2017). Data was imported into R using *flowCore* (Ellis et al., 2019). Data was filtered to
683 remove potential cell debris, cell aggregates and contaminants by constructing two gates,
684 one based on forward and side scatter and a second based on GFP and a violet (405nm)
685 excitation, 670/30 emission channel. GFP and mCherry measurements were normalized
686 by forward scatter. Presented data encompass 376 wells with a range of 127-8905 events
687 per well after filtering (median: 7095.5; 95% of samples have over 4000 events). For
688 fitting hill equations, we used the *drm* function in the package *drc* (Ritz et al., 2015)
689 using robust median estimation. mCherry measurements were log10 transformed and
690 fitted to a four-parameter log-logistic function with a parameterization converting the
691 natural log of the half-max value into a parameter. For Wor1-GFP, only data from
692 progesterone concentrations less than 2nM were used for fitting.
693
694
695 Acknowledgments
696
697 We thank members of the Johnson lab, in particular Matt Lohse and Kyle Fowler for
698 helpful discussions and Ananda Mendoza for technical support. We thank David
699 Gresham, Kerry Geiler-Samerotte, Mariana Gomez Schiavon and Ranen Aviner for
700 advice and the lab of Hana El-Samad and Dmitri Petrov for providing reagents. This
701 investigation has been aided by a grant from The Jane Coffin Childs Memorial Fund for
702 Medical Research (to N.Z.).
703
704

References

Acar, M., Mettetal, J. T., & van Oudenaarden, A. (2008). Stochastic switching as a survival strategy in fluctuating environments. *Nature Genetics*, *40*(4), 471–475. https://doi.org/10.1038/ng.110

Ackers, G. K., Johnson, A. D., & Shea, M. A. (1982). Quantitative model for gene regulation by lambda phage repressor. *Proceedings of the National Academy of Sciences*, *79*(4), 1129–1133. https://doi.org/10.1073/pnas.79.4.1129

Alon, U. (2007). Network motifs: Theory and experimental approaches. *Nature Reviews Genetics*, *8*(6), 450–461. https://doi.org/10.1038/nrg2102

Aranda-Díaz, A., Mace, K., Zuleta, I., Harrigan, P., & El-Samad, H. (2017). Robust Synthetic Circuits for Two-Dimensional Control of Gene Expression in Yeast. *ACS Synthetic Biology*, *6*(3), 545–554. https://doi.org/10.1021/acssynbio.6b00251

Bergen, M. S., Voss, E., & Soll, D. R. (1990). Switching at the cellular level in the white—Opaque transition of Candida albicans. *Journal of General Microbiology*, *136*(10), 1925–1936. https://doi.org/10.1099/00221287-136-10-1925

Boija, A., Klein, I. A., Sabari, B. R., Dall'Agnese, A., Coffey, E. L., Zamudio, A. V., Li, C. H., Shrinivas, K., Manteiga, J. C., Hannett, N. M., Abraham, B. J., Afeyan, L. K., Guo, Y. E., Rimel, J. K., Fant, C. B., Schuijers, J., Lee, T. I., Taatjes, D. J., & Young, R. A. (2018). Transcription Factors Activate Genes through the Phase-Separation Capacity of Their Activation Domains. *Cell*, *175*(7), 1842-1855.e16. https://doi.org/10.1016/j.cell.2018.10.042

Brachmann, C. B., Davies, A., Cost, G. J., Caputo, E., Li, J., Hieter, P., & Boeke, J. D. (1998). Designer deletion strains derived from Saccharomyces cerevisiae S288C:

A useful set of strains and plasmids for PCR-mediated gene disruption and other applications. *Yeast (Chichester, England)*, *14*(2), 115–132. https://doi.org/10.1002/(SICI)1097-0061(19980130)14:2<115::AID-YEA204>3.0.CO;2-2

Buchler, N. E., & Cross, F. R. (2009). Protein sequestration generates a flexible ultrasensitive response in a genetic network. *Molecular Systems Biology*, *5*(1), 272. https://doi.org/10.1038/msb.2009.30

Burz, D. S. (1998). Cooperative DNA-binding by Bicoid provides a mechanism for threshold-dependent gene activation in the Drosophila embryo. *The EMBO Journal*, *17*(20), 5998–6009. https://doi.org/10.1093/emboj/17.20.5998

Çağatay, T., Turcotte, M., Elowitz, M. B., Garcia-Ojalvo, J., & Süel, G. M. (2009). Architecture-Dependent Noise Discriminates Functionally Analogous Differentiation Circuits. *Cell*, *139*(3), 512–522. https://doi.org/10.1016/j.cell.2009.07.046

Chickarmane, V., Troein, C., Nuber, U. A., Sauro, H. M., & Peterson, C. (2006). Transcriptional Dynamics of the Embryonic Stem Cell Switch. *PLoS Computational Biology*, *2*(9), e123. https://doi.org/10.1371/journal.pcbi.0020123

Ellis, B., Haaland, P., Hahne, F., Meur, N. L., Gopalakrishnan, N., Spidlen, J., Jiang, M., & Finak, G. (2019). *FlowCore: FlowCore: Basic structures for flow cytometry data*.

Ene, I. V., Lohse, M. B., Vladu, A. V., Morschhäuser, J., Johnson, A. D., & Bennett, R. J. (2016). Phenotypic Profiling Reveals that *Candida albicans* Opaque Cells Represent a Metabolically Specialized Cell State Compared to Default White

751 Cells. *MBio*, *7*(6), e01269-16, /mbio/7/6/e01269-16.atom.
752 https://doi.org/10.1128/mBio.01269-16
753 Ferrell, J. E. (2002). Self-perpetuating states in signal transduction: Positive feedback,
754 double-negative feedback and bistability. *Current Opinion in Cell Biology*, *14*(2),
755 140–148. https://doi.org/10.1016/S0955-0674(02)00314-9
756 Ferrell, J. E., & Ha, S. H. (2014). Ultrasensitivity part III: Cascades, bistable switches,
757 and oscillators. *Trends in Biochemical Sciences*, *39*(12), 612–618.
758 https://doi.org/10.1016/j.tibs.2014.10.002
759 Frazer, C., Staples, M. I., Kim, Y., Hirakawa, M., Dowell, M. A., Johnson, N. V.,
760 Hernday, A. D., Ryan, V. H., Fawzi, N. L., Finkelstein, I. J., & Bennett, R. J.
761 (2020). Epigenetic cell fate in Candida albicans is controlled by transcription
762 factor condensates acting at super-enhancer-like elements. *Nature Microbiology*,
763 *5*(11), 1374–1389. https://doi.org/10.1038/s41564-020-0760-7
764 Gardner, T. S., Cantor, C. R., & Collins, J. J. (2000). Construction of a genetic toggle
765 switch in Escherichia coli. *Nature*, *403*(6767), 339–342.
766 https://doi.org/10.1038/35002131
767 Graham, T. G. W., Tabei, S. M. A., Dinner, A. R., & Rebay, I. (2010). Modeling bistable
768 cell-fate choices in the Drosophila eye: Qualitative and quantitative perspectives.
769 *Development*, *137*(14), 2265–2278. https://doi.org/10.1242/dev.044826
770 Guan, Z., & Liu, H. (2015). The *WOR 1* 5′ untranslated region regulates white-opaque
771 switching in *Candida albicans* by reducing translational efficiency: *WOR1* 5′
772 untranslated region. *Molecular Microbiology*, *97*(1), 125–138.
773 https://doi.org/10.1111/mmi.13014

Hahn, S., Hoar, E. T., & Guarente, L. (1985). Each of three “TATA elements” specifies a subset of the transcription initiation sites at the CYC-1 promoter of Saccharomyces cerevisiae. *Proceedings of the National Academy of Sciences of the United States of America*, *82*(24), 8562–8566.

Hernday, A. D., Lohse, M. B., Fordyce, P. M., Nobile, C. J., DeRisi, J. L., & Johnson, A. D. (2013). Structure of the transcriptional network controlling white-opaque switching in *Candida albicans*. *Molecular Microbiology*, *90*(1), 22–35. https://doi.org/10.1111/mmi.12329

Hooshangi, S., Thiberge, S., & Weiss, R. (2005). Ultrasensitivity and noise propagation in a synthetic transcriptional cascade. *Proceedings of the National Academy of Sciences*, *102*(10), 3581–3586. https://doi.org/10.1073/pnas.0408507102

Johnson, A. D., Poteete, A. R., Lauer, G., Sauer, R. T., Ackers, G. K., & Ptashne, M. (1981). λ Repressor and cro—Components of an efficient molecular switch. *Nature*, *294*(5838), 217–223. https://doi.org/10.1038/294217a0

Kaufmann, B. B., Yang, Q., Mettetal, J. T., & van Oudenaarden, A. (2007). Heritable Stochastic Switching Revealed by Single-Cell Genealogy. *PLoS Biology*, *5*(9), e239. https://doi.org/10.1371/journal.pbio.0050239

Kim, J., & Sudbery, P. (2011). Candida albicans, a major human fungal pathogen. *The Journal of Microbiology*, *49*(2), 171–177. https://doi.org/10.1007/s12275-011-1064-7

Kramer, B. P., Viretta, A. U., Baba, M. D.-E., Aubel, D., Weber, W., & Fussenegger, M. (2004). An engineered epigenetic transgene switch in mammalian cells. *Nature Biotechnology*, *22*(7), 867–870. https://doi.org/10.1038/nbt980

797 Kussell, E. (2005a). Bacterial Persistence: A Model of Survival in Changing
798 Environments. *Genetics*, *169*(4), 1807–1814.
799 https://doi.org/10.1534/genetics.104.035352
800 Kussell, E. (2005b). Phenotypic Diversity, Population Growth, and Information in
801 Fluctuating Environments. *Science*, *309*(5743), 2075–2078.
802 https://doi.org/10.1126/science.1114383
803 Lin, C.-H., Kabrawala, S., Fox, E. P., Nobile, C. J., Johnson, A. D., & Bennett, R. J.
804 (2013). Genetic Control of Conventional and Pheromone-Stimulated Biofilm
805 Formation in Candida albicans. *PLoS Pathogens*, *9*(4), e1003305.
806 https://doi.org/10.1371/journal.ppat.1003305
807 Lohse, M. B., Brenes, L. R., Ziv, N., Winter, M. B., Craik, C. S., & Johnson, A. D.
808 (2020). An Opaque Cell-Specific Expression Program of Secreted Proteases and
809 Transporters Allows Cell-Type Cooperation in *Candida albicans*. *Genetics*,
810 genetics.303613.2020. https://doi.org/10.1534/genetics.120.303613
811 Lohse, M. B., Ene, I. V., Craik, V. B., Hernday, A. D., Mancera, E., Morschhauser, J.,
812 Bennett, R. J., & Johnson, A. D. (2016). Systematic Genetic Screen for
813 Transcriptional Regulators of the Candida albicans White-Opaque Switch.
814 *Genetics*, *203*(4), 1679–1692. https://doi.org/10.1534/genetics.116.190645
815 Lohse, M. B., & Johnson, A. D. (2008). Differential phagocytosis of white versus opaque
816 Candida albicans by Drosophila and mouse phagocytes. *PloS One*, *3*(1), e1473.
817 https://doi.org/10.1371/journal.pone.0001473

Lohse, M. B., & Johnson, A. D. (2009). White–opaque switching in Candida albicans. *Current Opinion in Microbiology*, *12*(6), 650–654. https://doi.org/10.1016/j.mib.2009.09.010

Lohse, M. B., & Johnson, A. D. (2010). Temporal anatomy of an epigenetic switch in cell programming: The white-opaque transition of C. albicans. *Molecular Microbiology*, *78*(2), 331–343. https://doi.org/10.1111/j.1365-2958.2010.07331.x

Lohse, M. B., & Johnson, A. D. (2016). Identification and Characterization of Wor4, a New Transcriptional Regulator of White-Opaque Switching. *G3: Genes|Genomes|Genetics*, *6*(3), 721–729. https://doi.org/10.1534/g3.115.024885

Losick, R., & Desplan, C. (2008). Stochasticity and Cell Fate. *Science*, *320*(5872), 65–68. https://doi.org/10.1126/science.1147888

Maamar, H., & Dubnau, D. (2005). Bistability in *the Bacillus subtilis* K-state (competence) system requires a positive feedback loop: Bistability in *B. subtilis* competence. *Molecular Microbiology*, *56*(3), 615–624. https://doi.org/10.1111/j.1365-2958.2005.04592.x

McIsaac, R. S., Gibney, P. A., Chandran, S. S., Benjamin, K. R., & Botstein, D. (2014). Synthetic biology tools for programming gene expression without nutritional perturbations in Saccharomyces cerevisiae. *Nucleic Acids Research*, *42*(6), e48–e48. https://doi.org/10.1093/nar/gkt1402

Miller, M. G., & Johnson, A. D. (2002). White-opaque switching in Candida albicans is controlled by mating-type locus homeodomain proteins and allows efficient mating. *Cell*, *110*(3), 293–302.

840 Nguyen, N., Quail, M. M. F., & Hernday, A. D. (2017). An Efficient, Rapid, and
841 Recyclable System for CRISPR-Mediated Genome Editing in *Candida albicans*.
842 *MSphere*, *2*(2). https://doi.org/10.1128/mSphereDirect.00149-17
843 Noble, S. M., French, S., Kohn, L. A., Chen, V., & Johnson, A. D. (2010). Systematic
844 screens of a Candida albicans homozygous deletion library decouple
845 morphogenetic switching and pathogenicity. *Nature Genetics*, *42*(7), 590–598.
846 https://doi.org/10.1038/ng.605
847 Noble, S. M., & Johnson, A. D. (2005). Strains and Strategies for Large-Scale Gene
848 Deletion Studies of the Diploid Human Fungal Pathogen *Candida albicans*.
849 *Eukaryotic Cell*, *4*(2), 298–309. https://doi.org/10.1128/EC.4.2.298-309.2005
850 Norman, T. M., Lord, N. D., Paulsson, J., & Losick, R. (2015). Stochastic Switching of
851 Cell Fate in Microbes. *Annual Review of Microbiology*, *69*(1), 381–403.
852 https://doi.org/10.1146/annurev-micro-091213-112852
853 Park, B. O., Ahrends, R., & Teruel, M. N. (2012). Consecutive Positive Feedback Loops
854 Create a Bistable Switch that Controls Preadipocyte-to-Adipocyte Conversion.
855 *Cell Reports*, *2*(4), 976–990. https://doi.org/10.1016/j.celrep.2012.08.038
856 Phillips, G. N. (1997). Structure and dynamics of green fluorescent protein. *Current*
857 *Opinion in Structural Biology*, *7*(6), 821–827. https://doi.org/10.1016/S0959-
858 440X(97)80153-4
859 Porman, A. M., Alby, K., Hirakawa, M. P., & Bennett, R. J. (2011). Discovery of a
860 phenotypic switch regulating sexual mating in the opportunistic fungal pathogen
861 Candida tropicalis. *Proceedings of the National Academy of Sciences*, *108*(52),
862 21158–21163. https://doi.org/10.1073/pnas.1112076109

Ptashne, M. (2011). Principles of a switch. *Nature Chemical Biology*, *7*(8), 484–487. https://doi.org/10.1038/nchembio.611

Pujol, C., Daniels, K. J., Lockhart, S. R., Srikantha, T., Radke, J. B., Geiger, J., & Soll, D. R. (2004). The Closely Related Species Candida albicans and Candida dubliniensis Can Mate. *Eukaryotic Cell*, *3*(4), 1015–1027. https://doi.org/10.1128/EC.3.4.1015-1027.2004

R Core Team. (2019). *R: A Language and Environment for Statistical Computing*. R Foundation for Statistical Computing. https://www.R-project.org/

Raj, A., & van Oudenaarden, A. (2008). Nature, Nurture, or Chance: Stochastic Gene Expression and Its Consequences. *Cell*, *135*(2), 216–226. https://doi.org/10.1016/j.cell.2008.09.050

Ritz, C., Baty, F., Streibig, J. C., & Gerhard, D. (2015). Dose-Response Analysis Using R. *PLOS ONE*, *10*(12), e0146021. https://doi.org/10.1371/journal.pone.0146021

Rosen, J. M., & Jordan, C. T. (2009). The Increasing Complexity of the Cancer Stem Cell Paradigm. *Science*, *324*(5935), 1670–1673. https://doi.org/10.1126/science.1171837

Ryan, O. W., Skerker, J. M., Maurer, M. J., Li, X., Tsai, J. C., Poddar, S., Lee, M. E., DeLoache, W., Dueber, J. E., Arkin, A. P., & Cate, J. H. (2014). Selection of chromosomal DNA libraries using a multiplex CRISPR system. *ELife*, *3*, e03703. https://doi.org/10.7554/eLife.03703

Sánchez Alvarado, A., & Yamanaka, S. (2014). Rethinking Differentiation: Stem Cells, Regeneration, and Plasticity. *Cell*, *157*(1), 110–119. https://doi.org/10.1016/j.cell.2014.02.041

Santillán, M., & Mackey, M. C. (2008). Quantitative approaches to the study of bistability in the *lac* operon of *Escherichia coli*. *Journal of The Royal Society Interface*, *5*(suppl_1). https://doi.org/10.1098/rsif.2008.0086.focus

Sasse, C., Hasenberg, M., Weyler, M., Gunzer, M., & Morschhauser, J. (2013). White-Opaque Switching of Candida albicans Allows Immune Evasion in an Environment-Dependent Fashion. *Eukaryotic Cell*, *12*(1), 50–58. https://doi.org/10.1128/EC.00266-12

Schindelin, J., Arganda-Carreras, I., Frise, E., Kaynig, V., Longair, M., Pietzsch, T., Preibisch, S., Rueden, C., Saalfeld, S., Schmid, B., Tinevez, J.-Y., White, D. J., Hartenstein, V., Eliceiri, K., Tomancak, P., & Cardona, A. (2012). Fiji: An open-source platform for biological-image analysis. *Nature Methods*, *9*(7), 676–682. https://doi.org/10.1038/nmeth.2019

Smits, W. K., Kuipers, O. P., & Veening, J.-W. (2006). Phenotypic variation in bacteria: The role of feedback regulation. *Nature Reviews Microbiology*, *4*(4), 259–271. https://doi.org/10.1038/nrmicro1381

Sriram, K., Soliman, S., & Fages, F. (2009). Dynamics of the interlocked positive feedback loops explaining the robust epigenetic switching in Candida albicans. *Journal of Theoretical Biology*, *258*(1), 71–88. https://doi.org/10.1016/j.jtbi.2009.01.008

Stockwell, S. R., Landry, C. R., & Rifkin, S. A. (2015). The yeast galactose network as a quantitative model for cellular memory. *Molecular BioSystems*, *11*(1), 28–37. https://doi.org/10.1039/C4MB00448E

908 Sudbery, P., Gow, N., & Berman, J. (2004). The distinct morphogenic states of Candida
909 albicans. *Trends in Microbiology*, *12*(7), 317–324.
910 https://doi.org/10.1016/j.tim.2004.05.008
911 Tuch, B. B., Mitrovich, Q. M., Homann, O. R., Hernday, A. D., Monighetti, C. K., De La
912 Vega, F. M., & Johnson, A. D. (2010). The Transcriptomes of Two Heritable Cell
913 Types Illuminate the Circuit Governing Their Differentiation. *PLoS Genetics*,
914 *6*(8), e1001070. https://doi.org/10.1371/journal.pgen.1001070
915 Van den Bergh, B., Fauvart, M., & Michiels, J. (2017). Formation, physiology, ecology,
916 evolution and clinical importance of bacterial persisters. *FEMS Microbiology*
917 *Reviews*, *41*(3), 219–251. https://doi.org/10.1093/femsre/fux001
918 Wernet, M. F., Mazzoni, E. O., Çelik, A., Duncan, D. M., Duncan, I., & Desplan, C.
919 (2006). Stochastic spineless expression creates the retinal mosaic for colour
920 vision. *Nature*, *440*(7081), 174–180. https://doi.org/10.1038/nature04615
921 Wickham, H. (2017). *tidyverse: Easily Install and Load the "Tidyverse."*
922 https://CRAN.R-project.org/package=tidyverse
923 Winston, F., Dollard, C., & Ricupero-Hovasse, S. L. (1995). Construction of a set of
924 convenientsaccharomyces cerevisiae strains that are isogenic to S288C. *Yeast*,
925 *11*(1), 53–55. https://doi.org/10.1002/yea.320110107
926 Wu, M., Su, R.-Q., Li, X., Ellis, T., Lai, Y.-C., & Wang, X. (2013). Engineering of
927 regulated stochastic cell fate determination. *Proceedings of the National Academy*
928 *of Sciences*, *110*(26), 10610–10615. https://doi.org/10.1073/pnas.1305423110

929 Yang, F., Moss, L. G., & Phillips, G. N. (1996). The molecular structure of green
930 fluorescent protein. *Nature Biotechnology*, *14*(10), 1246–1251.
931 https://doi.org/10.1038/nbt1096-1246
932 Zacharias, D. A. (2002). Partitioning of Lipid-Modified Monomeric GFPs into
933 Membrane Microdomains of Live Cells. *Science*, *296*(5569), 913–916.
934 https://doi.org/10.1126/science.1068539
935 Zordan, R. E., Galgoczy, D. J., & Johnson, A. D. (2006). Epigenetic properties of white-
936 opaque switching in Candida albicans are based on a self-sustaining
937 transcriptional feedback loop. *Proceedings of the National Academy of Sciences*,
938 *103*(34), 12807–12812. https://doi.org/10.1073/pnas.0605138103
939 Zordan, R. E., Miller, M. G., Galgoczy, D. J., Tuch, B. B., & Johnson, A. D. (2007).
940 Interlocking Transcriptional Feedback Loops Control White-Opaque Switching in
941 Candida albicans. *PLoS Biology*, *5*(10), e256.
942 https://doi.org/10.1371/journal.pbio.0050256
943
944

Table S1

White to Opaque switching

Genotype	Plates	Colonies	Sectors	Percent Switch	Fold Change
WT	11 (3,3,5)	1340	17	1.27 (+/- 0.306)	-
Wor1 motif deletion	11 (3,3,5)	1790	8	0.447 (+/- 0.158)	2.83 down
Wor1-GFP	11 (3,3,5)	948	491	51.8 (+/- 1.62)	40.8 up
Wor1-mGFP	11 (3,3,5)	1603	31	1.93 (+/- 0.344)	1.52 up

Opaque to White switching

Genotype	Plates	Colonies	Sectors	Percent Switch	Fold Change
WT	11 (3,3,5)	1926	87	4.52 (+/- 0.473)	-
Wor1 motif deletion	11 (3,3,5)	1159	224	19.3 (+/- 1.16)	4.28 up
Wor1-GFP	11 (3,3,5)	1633	0	<0.06	>75 down
Wor1-mGFP	11 (3,3,5)	1707	52	3.05 (+/- 0.42)	1.48 down

Table S1 – Switching frequencies
Switching frequencies as calculated by counting sectors on colonies grown on solid ager plates. Data comes from three independent experiments containing multiple plates per strain. Numbers of colonies and sectors are pooled across plates. The percent of colonies with at least one sector is calculated. Standard error is the standard error of a sample proportion ($\sqrt{[p (1-p) / n]}$).

Figure S1

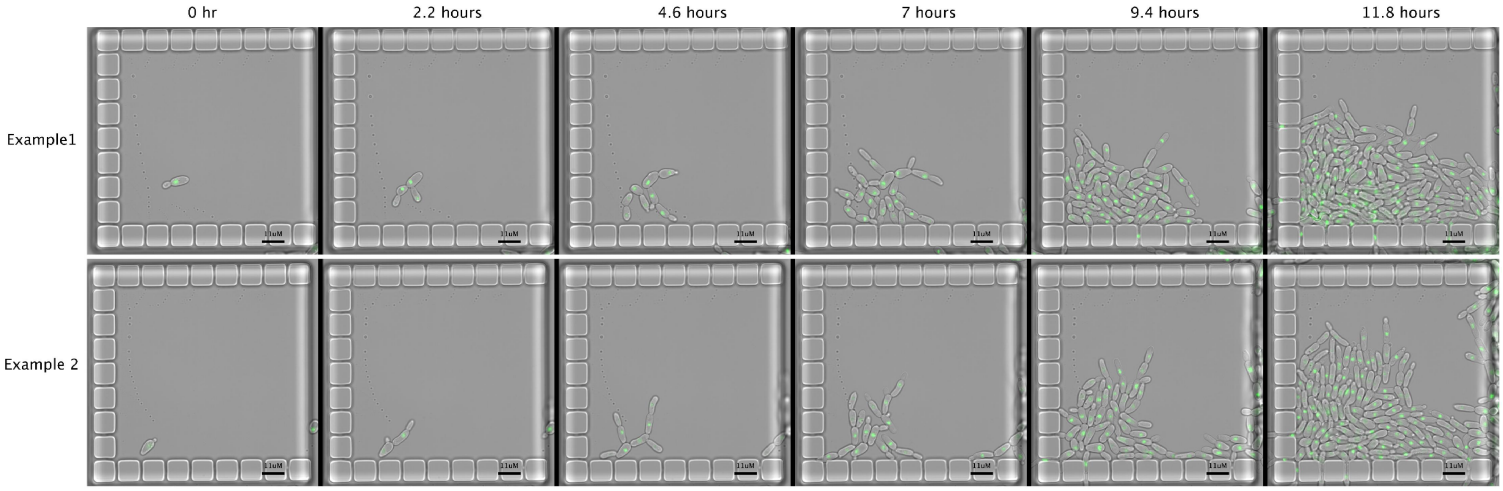

Figure S1 – Opaque cell growth in microfluidic traps
Two examples of microfluidic traps with growing opaque cells. Strain contains Wor1-GFP fusion protein.

Figure S2

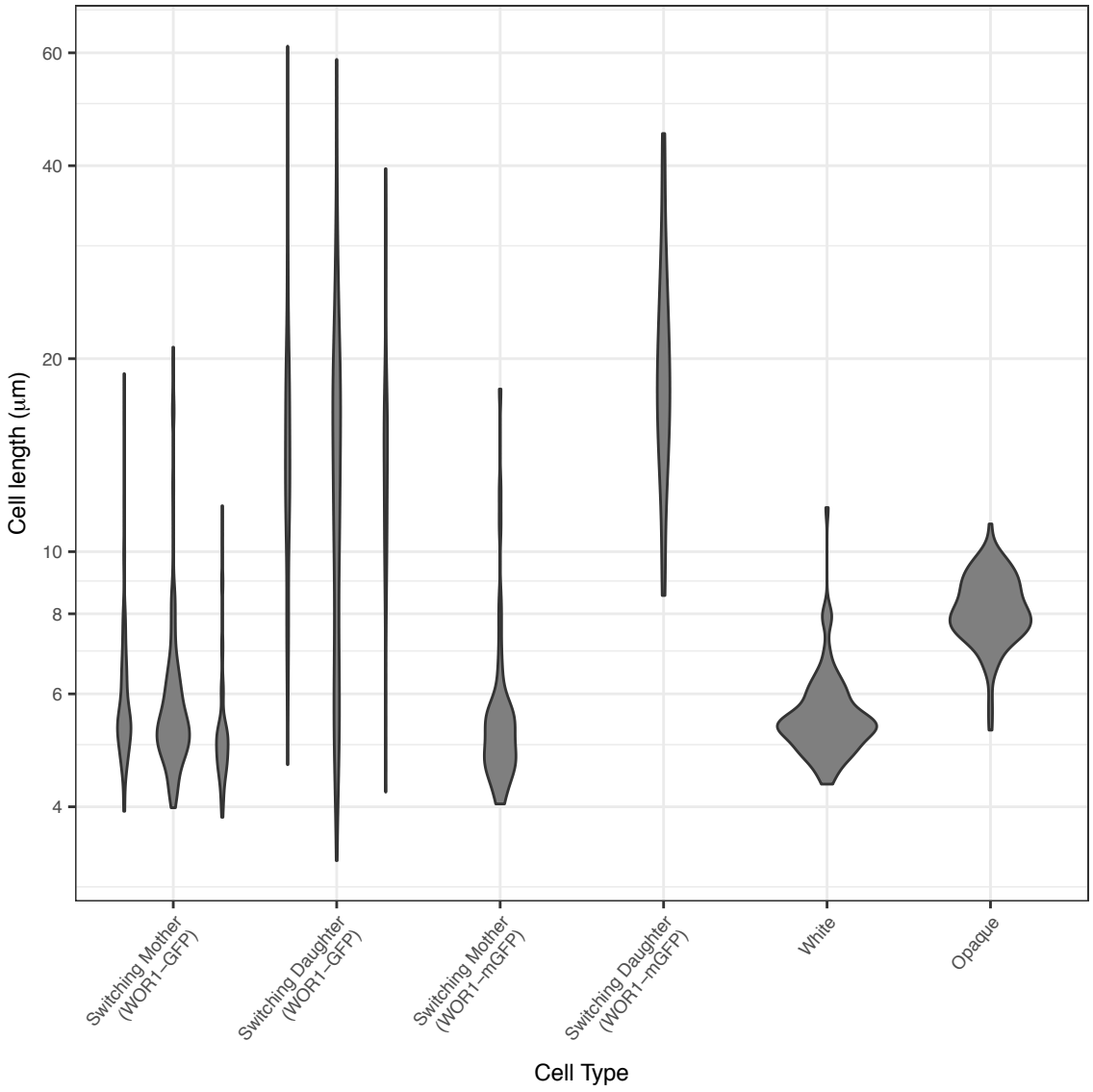

Figure S2 – Cell length distributions
Cell length distributions (violin plots) of different cell types, including switching cells containing Wor1-mGFP. For the Wor1-GFP strain, data comes from three independent experiments that were pooled in Figure 2.

Figure S3

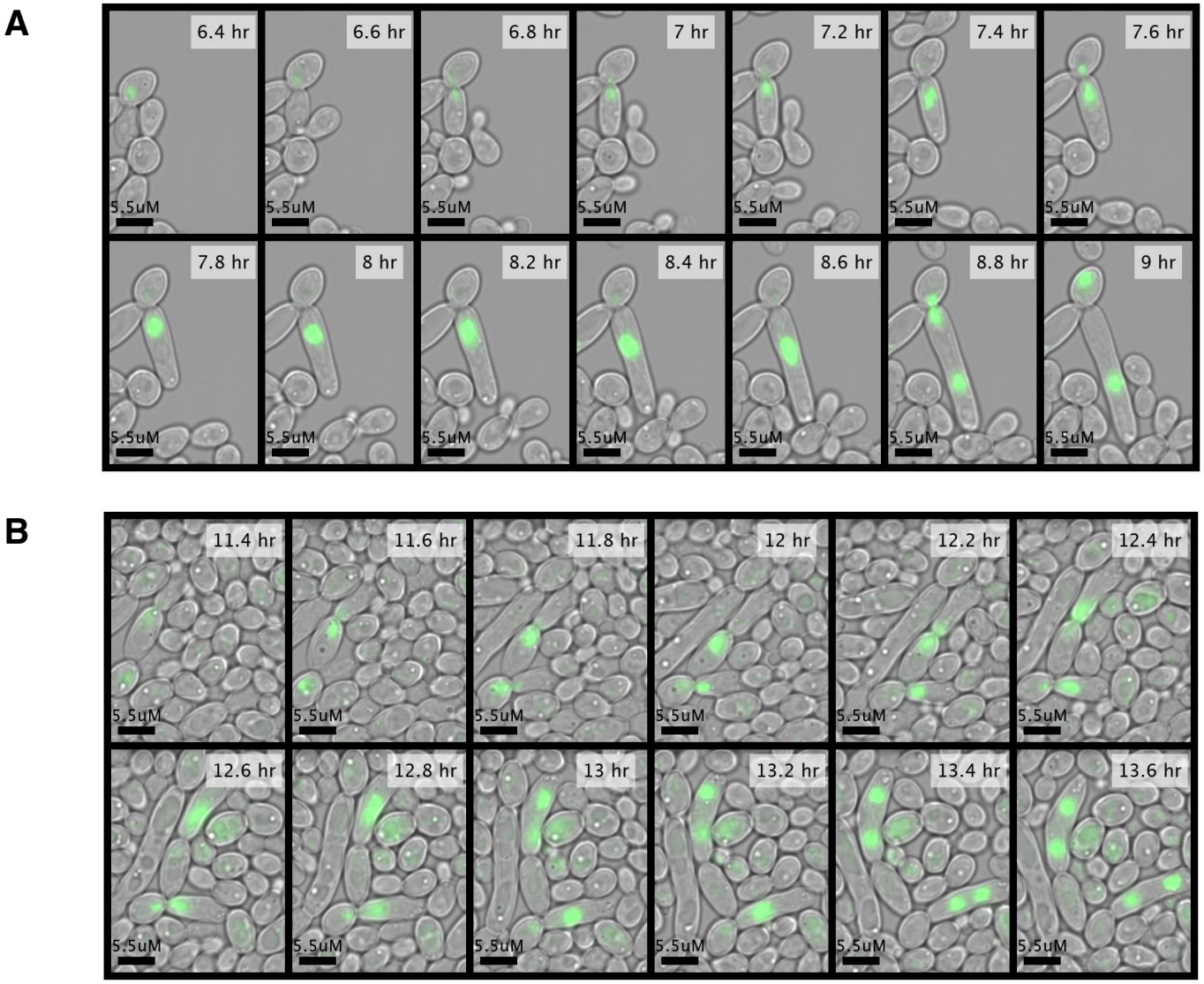

Figure S3 – Nucleus loss during mitosis in switching cells
A) Representative example of a cell division where the mother cell nucleus enters the elongated daughter cell but returns to the mother cell. Strain contains Wor1-GFP fusion protein. B) Representative example of cell divisions where the mother cell nucleus enters the elongated daughter cell and remains in the daughter cell, creating a polyploid cell. There are two cell divsions with this pattern in this example. Strain contains Wor1-GFP fusion protein.

Figure S4

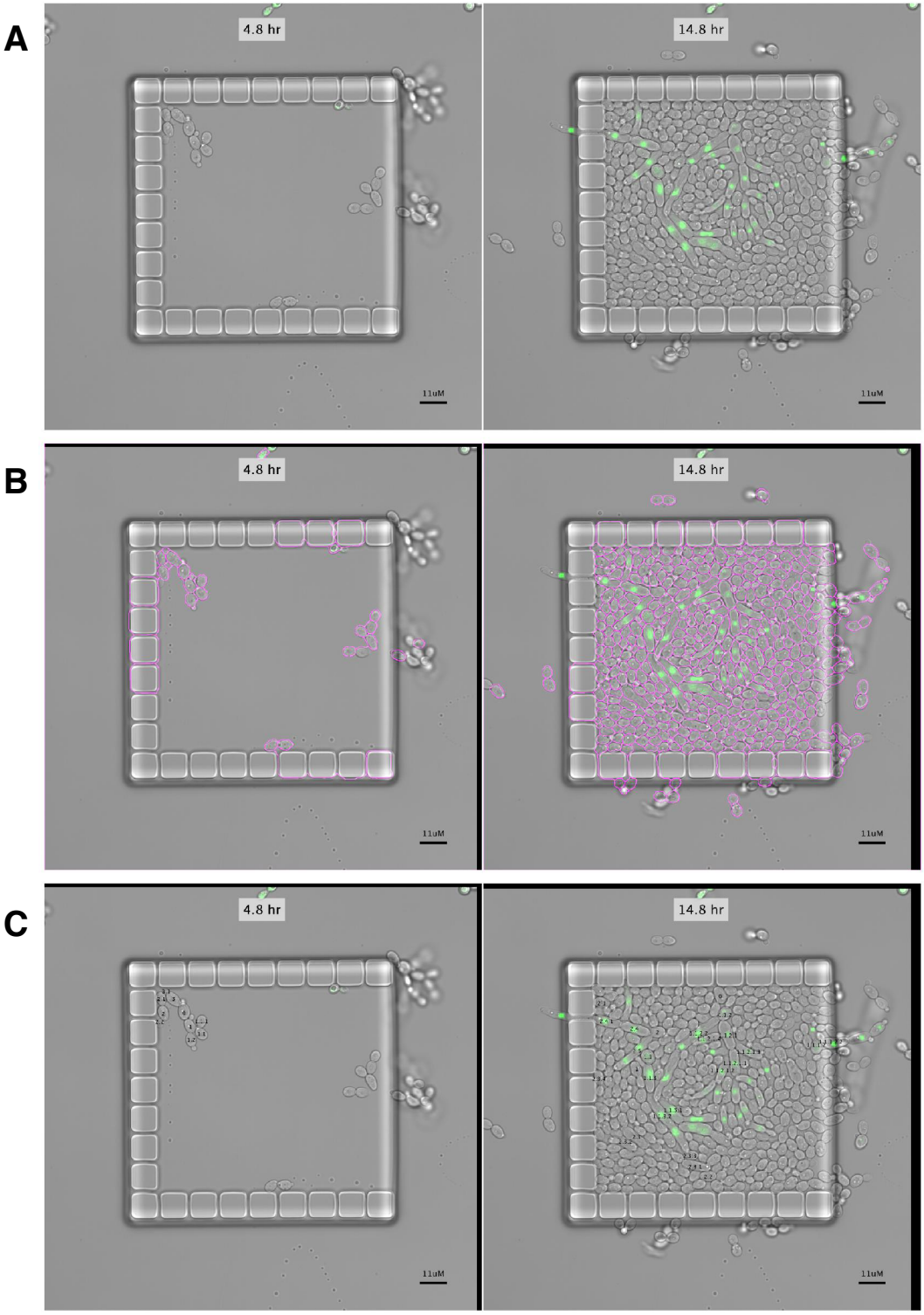

Figure S4 – Semi-automated image analysis pipeline
A) Representative original images of two time-points for one field. B) Same images as (A) after adjustment for (x,y) movement (note black regions at image edge) and automated segmentation of cells (magenta colored lines defining cell borders). C) Same images as (A) and (B) with overlay of manually defined cell identities, pedigree information is explicitly encoded in cell names (e.g., cell “2.1” is the first daughter of cell “2” which in turn is the second daughter of cell “0”).

Figure S5

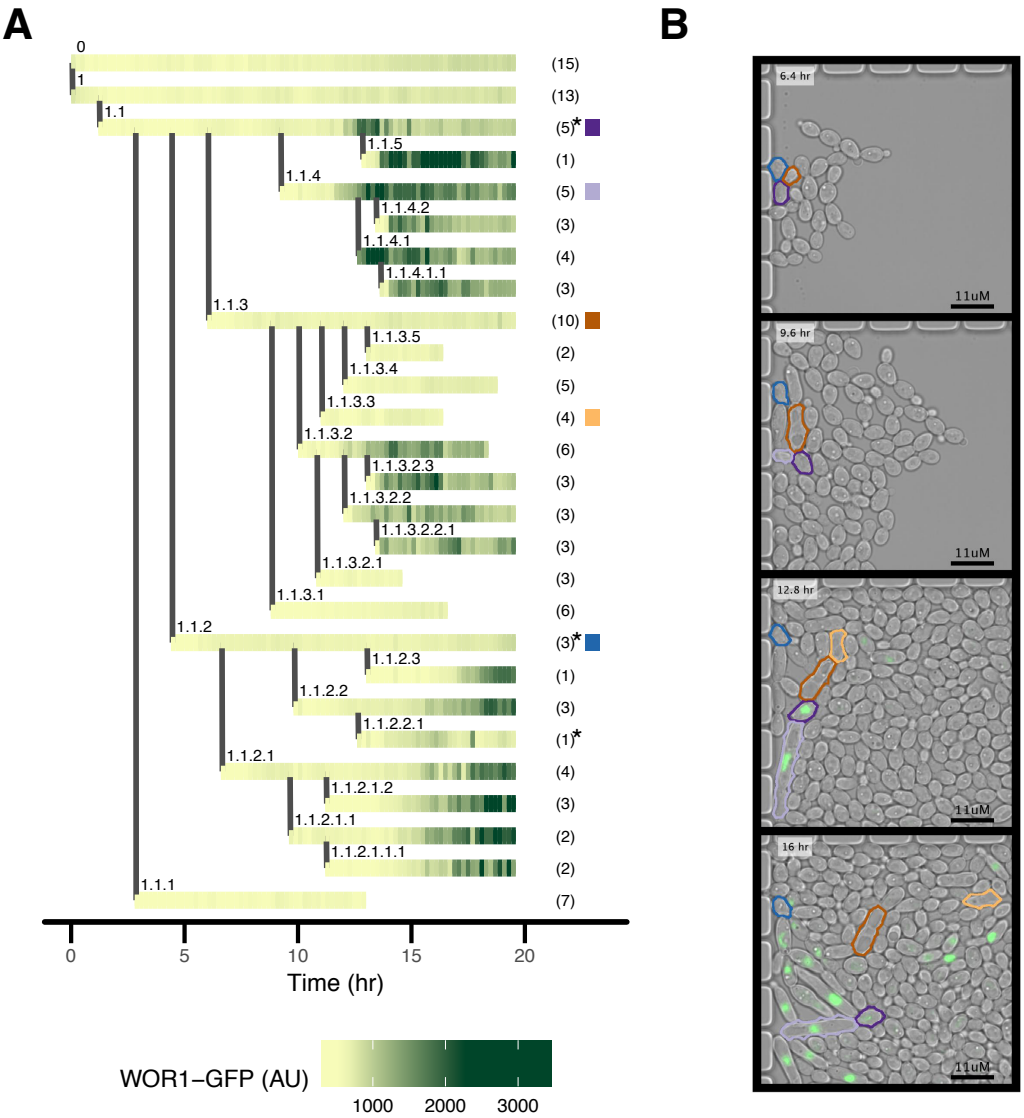

Figure S5 – Mixed fate pedigree example, Wor1-GFP
A) Representative pedigree in which multiple groups of cells activated Wor1. Horizontal lines represent single cells; vertical lines represent budding of a daughter cell. Every horizontal line is made up of small tiles colored by Wor1-GFP fluorescence. Numbers within parentheses on the right of the pedigree represent the number of budded daughter cells per cell within the time period shown; not all daughters are depicted in the pedigree. An asterisk represents that the cell lost its nucleus to its daughter cell. Colored square tiles single out particular cells that are depicted in (B). B) Subset of images representing data shown in (A). Particular cells are outlined in colors corresponding to (A). Cell outlines are based on automated image analysis.

Figure S6

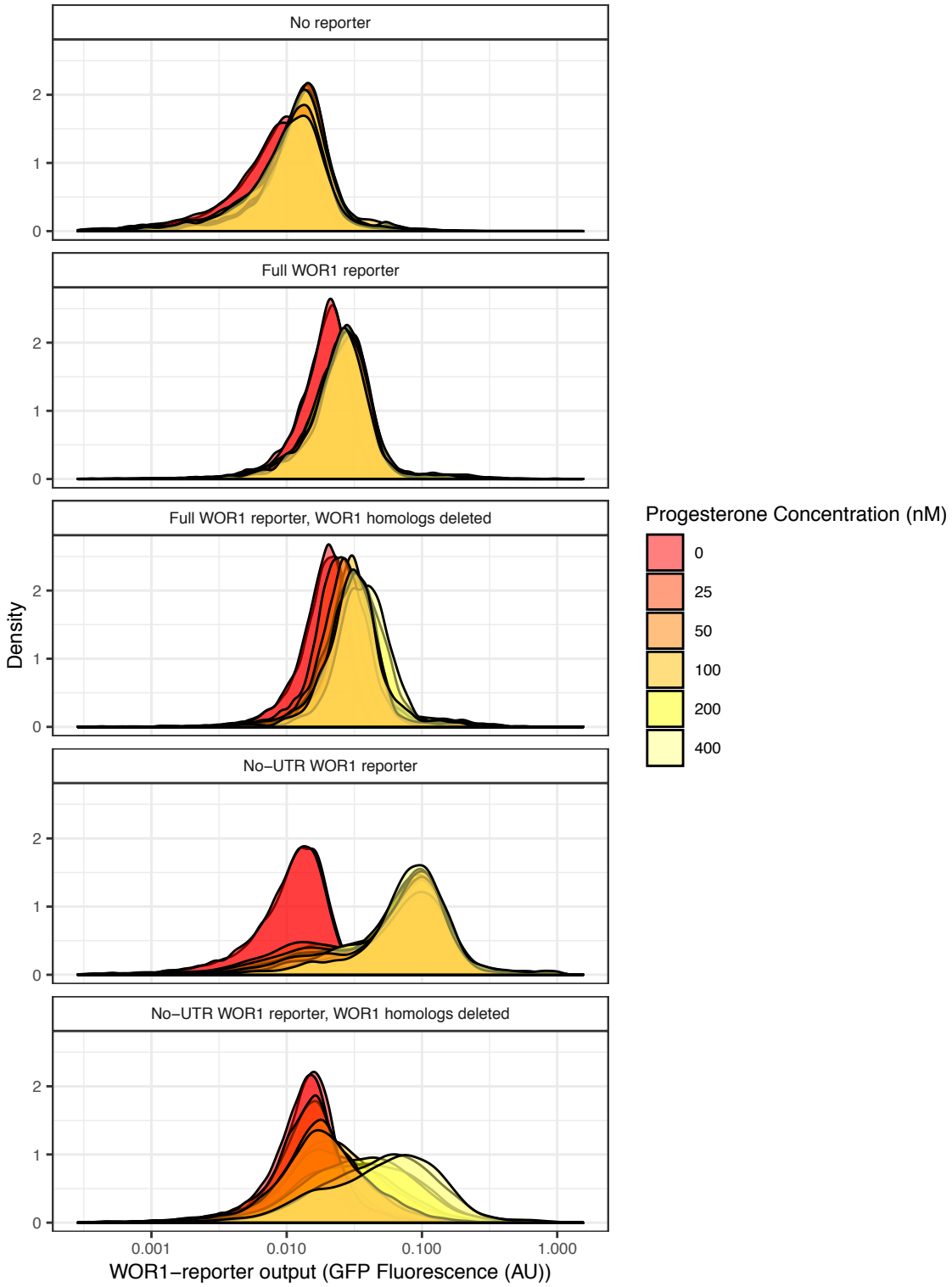

Figure S6 - Alternative Wor1 transcriptional reporters in S. cerevisiae
Distributions of Wor1 transcriptional reporters; all strains shown are inducing Wor1 protein with increasing progesterone concentrations and were independently constructed from the strains shown in the main text. “Full” reporter contains both the Wor1 7KB control region and promoter and the Wor1 2KB 5’UTR. The “No-UTR” reporter contains the Wor1 control region and the Cyc1 core promoter and 5’UTR as explained in the methods section.

Figure S7

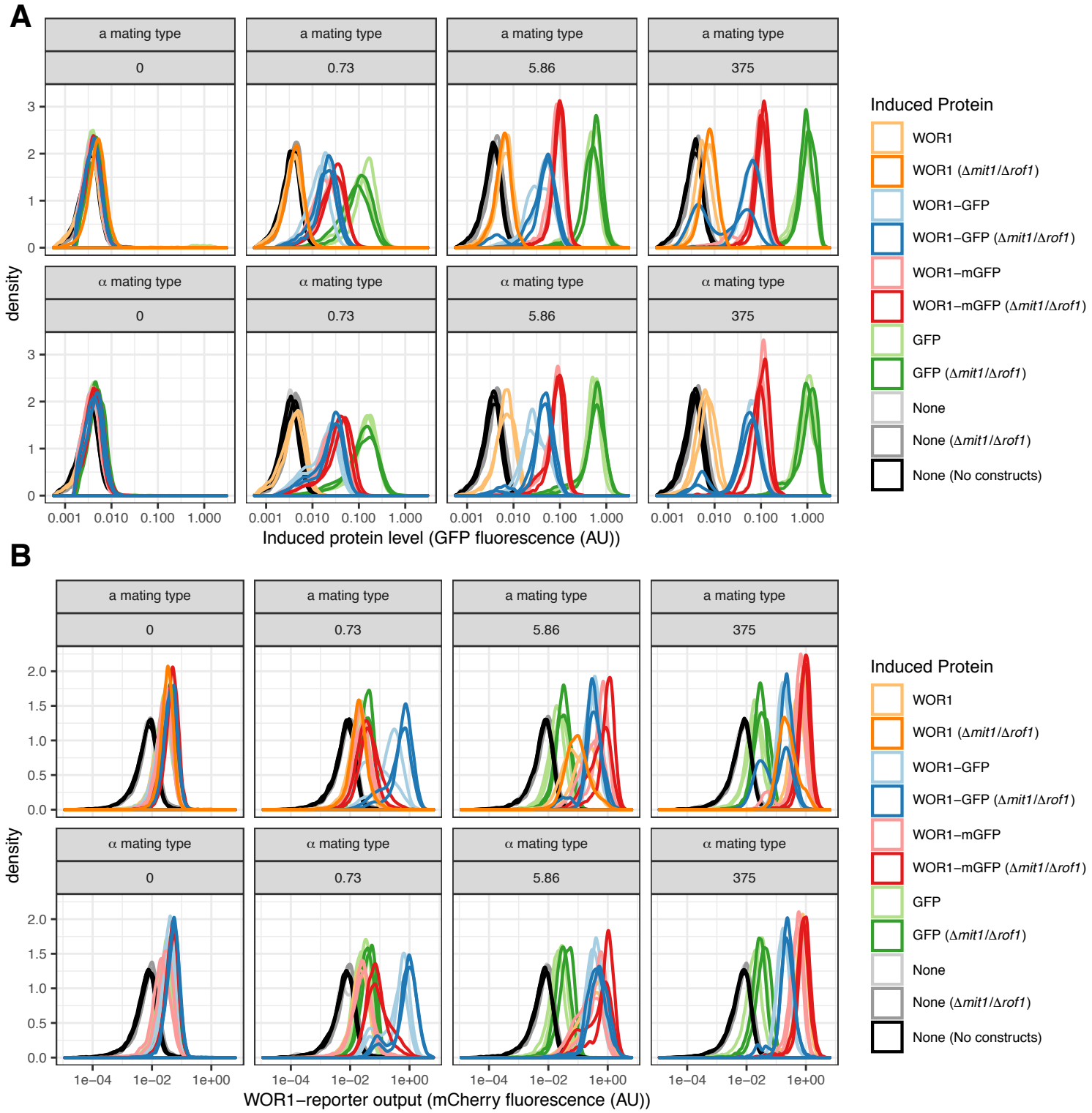

Figure S7 - Distributions of Wor1 protein and reporter levels
Distributions of GFP (A) and mCherry (B) fluorescence; data is shown for all strains in a subset of 4 hormone concentrations (nM progesterone). Note bimodal distributions of GFP fluorescence when inducing Wor1-GFP at high hormone concentrations in (A). Note low-level expression of the Wor1 transcriptional reporter compared to auto-fluorescence in (B).

Figure S8

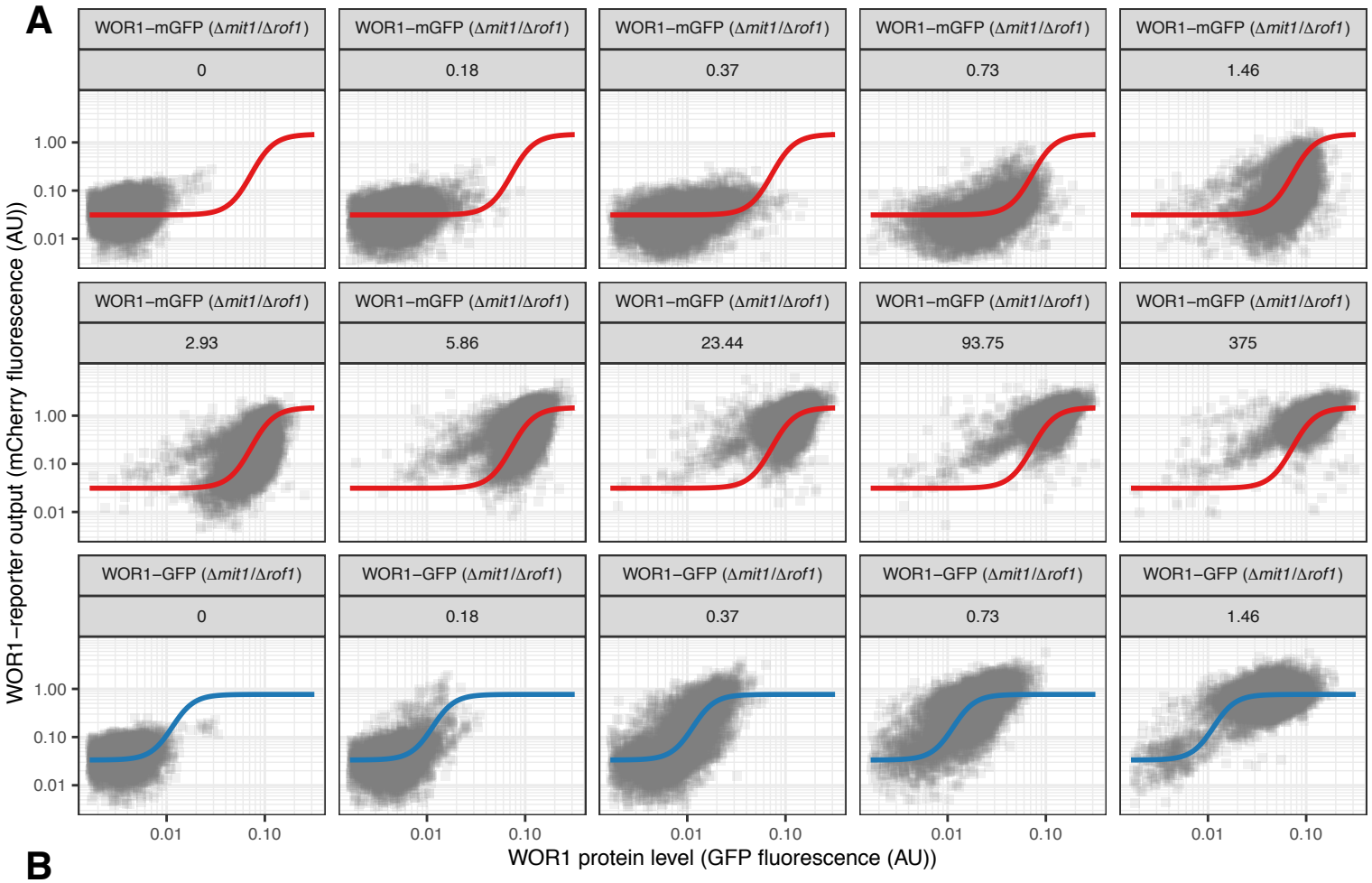

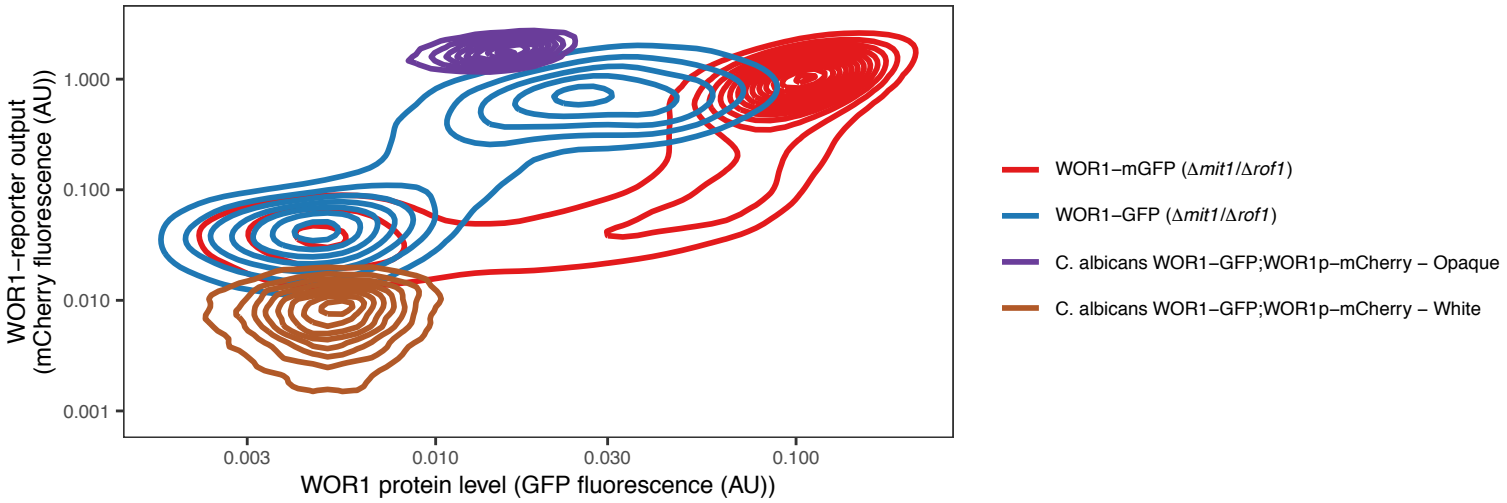

Figure S8 – Distributions of Wor1 protein and reporter levels
A) Same data as Figure 5C, separated by hormone concentration (nM progesterone). B) 2D density plots of flow cytometry data. S. cerevisiae Wor1-GFP and Wor1-mGFP data (same as A) are shown alongside data for white and opaque C. albicans cells containing a Wor1-GFP fusion protein and a transcriptional reporter encompassing the 7KB control region of Wor1 followed by mCherry (no 5'UTR sequence).